Journal of South American Earth Sciences 45 (2013) 6–23

Contents lists available at SciVerse ScienceDirect

Journal of South American Earth Sciences

journal homepage: www.elsevier.com/locate/jsames

Late Eocene to Early Miocene Andean uplift inferred from detrital zircon fission track and U–Pb dating of Cenozoic forearc sediments (15–18°S)

A. Decou[a,*], H. von Eynatten[a], I. Dunkl[a], D. Frei[b], G. Wörner[a]

[a] Geowissenschaftliches Zentrum der Universität Göttingen, Goldschmidtstr. 3, D-37077 Göttingen, Germany
[b] Department of Earth Sciences, Stellenbosch University, Private Bag X1, 7602 Matieland, South Africa

ARTICLE INFO

Article history:
Received 2 March 2012
Accepted 13 February 2013

Keywords:
Central Andes
Tertiary
Crustal thickening
Provenance analysis
Detrital zircon
Fission track thermochronology
U–Pb dating

ABSTRACT

Timing, amount, and mechanisms of uplift in the Central Andes have been a matter of debate in the last decade. Our study is based on the Cenozoic Moquegua Group deposited in the forearc basin between the Western Cordillera and the Coastal Cordillera in southern Peru from ~50 to ~4 Ma. The Moquegua Group consists mainly of mud-flat to fluvial siliciclastic sediments with upsection increasing grain size and volcanic intercalations. Detrital zircon U–Pb dating and fission track thermochronology allow us to refine previous sediment provenance models and to constrain the timing of Late Eocene to Early Miocene Andean uplift. Uplift-related provenance and facies changes started around 35 Ma and thus predate major voluminous ignimbrite eruptions that started at ~25 by up to 10 Ma. Therefore magmatic addition to the crust cannot be an important driving factor for crustal thickening and uplift at Late Eocene to Early Oligocene time. Changes in subduction regime and the subducting plate geometry are suggested to control the formation of significant relief in the area of the future Western Cordillera which acts as an efficient large-scale drainage divide between Altiplano and forearc from at least 15.5 to 19°S already at ~35 Ma. The model integrates the coincidence of (i) onset of provenance change no later than 35 Ma, (ii) drastic decrease in convergence rates at ~40, (iii) a flat-subduction period at around ~40 to ~30 Ma leading to strong interplate coupling, and (iv) strong decrease in volcanic activity between 45 and 30 Ma.

1. Introduction

The Central Andes presently form the largest mountain chain built by subduction processes in one of the most intensely thickened region of the South American continent (Sempere et al., 2008). Since Jurassic time the oceanic Nazca plate is being subducted beneath the South American continent. Ongoing subduction, crustal shortening (Isacks, 1988; Allmendinger et al., 1997) and – to a minor extend – magma addition have lead to the construction of the Central Andes edifice with its up to 70 km thick continental crust. However, despite long lasting subduction, the uplift is generally considered to have not started before middle Eocene time (Isacks, 1988; Allmendinger et al., 1997; Sempere et al., 2008). The elevation reached during this first pulse of uplift (~45–20 Ma; Anders et al., 2002; Gillis et al., 2006) is strongly debated (Gregory-Wodzicki, 2000; Sempere et al., 2008). A second pulse of uplift has been recognized to be late Miocene in age starting at ~10 Ma (Lamb and Hoke, 1997; Schildgen et al., 2007; Thouret et al., 2007; Garzione et al., 2008; Sempere et al., 2008). Despite its fundamental role for surface uplift, processes which lead to ~70 km thick crust are strongly debated. Tectonic shortening is widely accepted to be responsible for initial crustal thickening (Oncken et al., 2006). However, nearly no shortening occurred in the western Andean margin of the Central Andes since more than 10 Ma (Isacks, 1988; Wörner et al., 2000b, 2002; Oncken et al., 2006; Sempere and Jacay, 2007). Molnar and Garzione (2007) and (Garzione et al., 2007, 2008) proposed that delamination of dense lithospheric material into the mantle was responsible for uplift. However, delamination should be a consequence of thickening (Kay and Mahlburg-Kay, 1991) and cannot be its cause. Moreover, no magmatic products typical of this process are actually known from the region (Kay and Mahlburg Kay, 1993; Kay and Coira, 2009; Mamani et al., 2010). Alternatively, various authors (e.g. Meissner and Mooney, 1998; Babeyko et al., 2002; Beck and Zandt, 2002; Wörner et al., 2002; Husson and Sempere, 2003; Oncken et al., 2006) suggested that large-scale lateral flow of ductile lower crust may have contributed significantly to crustal thickening in the west with regional tilt on the Western Andean margin and limited upper crustal shortening.

* Corresponding author. Present address: CASP, West Building, 181a Huntingdon Road, Cambridge CB3 0DH, UK.
E-mail address: audrey.decou@casp.cam.ac.uk (A. Decou).

0895-9811/$ – see front matter
http://dx.doi.org/10.1016/j.jsames.2013.02.003

Shortly before and during Cenozoic crustal thickening a large forearc basin developed between the Coastal Cordillera and the Western Cordillera in Southern Peru and Northern Chile (Fig. 1). The basin is filled by continental siliciclastic and volcaniclastic sediments named the Moquegua Group in southern Peru which are relatively well dated due to several ignimbrite and tuff intercalations (Quang and Clark, 2005; Thouret et al., 2007, and references therein). The entire sequence is considered to range in age from ~50 to ~4 Ma (Roperch et al., 2006) and forms an excellent archive of the Cenozoic geologic and topographic evolution of the area (Decou et al., 2011). Provenance analysis of such archives allows for reconstructing tectonic processes in the hinterland as well as climatic, hydrological and topographic changes through time and space (e.g. von Eynatten, 2003; Najman, 2006; Carrapa, 2010). However, the potential of advanced provenance analysis techniques applied to the Cenozoic forearc sediments of southern Peru and northern Chile to reconstruct the geologic and uplift history of the Central Andes has not been used until recent time (Pinto et al., 2007; Decou et al., 2011; Wotzlaw et al., 2011).

The purpose of this paper is to evaluate the varying sediment sources and dispersal patterns through time at the western flank of the growing Andean orogen in southern Peru (15–18°S) using geochronological and thermochronological methods. Specifically, we apply U–Pb as well as fission track dating of detrital zircon grains to infer both crystallisation and cooling ages from the respective source areas of the Moquegua Group. The main focus is on the first (Eocene to Early Miocene) phase of uplift and relief formation which is much less well constrained compared to the second Late Miocene uplift. To ensure precise provenance evaluation we will first summarize previously published geochronological information on potential source rocks. This is quite complex due to the long-lasting accretion history of the South American continent during Proterozoic time (Bahlburg et al., 2009) as well as numerous younger magmatic events (Mamani et al., 2010). Data compilation will be completed by own source rock U–Pb data obtained for this study, before going into the details of the Cenozoic Moquegua basin sediments. The thermochronological data will be used to track the thermal imprint of arc volcanism in the hinterland and as additional constraint on sediment provenance. The resulting provenance model integrates previously published data on heavy minerals and mineral chemistry of Moquegua Group (Decou et al., 2011), and is used to constrain the Eocene to Miocene crustal thickening and uplift history for the Central Andes.

2. Geological setting

The Andean belt is divided into Northern, Central and Southern Andes (Fig. 1a). The Central Andes are composed of the Northern Central Andes, the Central Andean Orocline and the Southern Central Andes. The Central Andean Orocline is composed of four main geomorphologic features, from southwest to northeast, the Coastal Cordillera, Western Cordillera, Altiplano and Eastern Cordillera (Fig. 1b). The main characteristic of the Central Andean Orocline is its ~70 km thick crust (Lyon-Caen et al., 1985; Beck et al., 1996; Yuan et al., 2002). Our study area is located at the western margin of the northwestern segment of the Central Andean Orocline in southern Peru (74–70°W, 15–18°S); situated in the forearc between the Coastal and Western Cordilleras (Fig. 1b).

The Andes represent the locus of continued plate convergence through much of Phanerozoic time with the accretion of different cratonic blocks and terrains (Ramos, 1988; Bahlburg et al., 2009) (Fig. 2). The Andean cycle started about 200 Ma ago (Cawood, 2005) and is related to the initiation of the Nazca plate subduction under the South American continent. Pardo-Casas and Molnar (1987) and Somoza (1998) reconstructed the convergence history of the Nazca and South American plates since late Cretaceous time. Convergence rate rapidly increased between ~60 Ma and ~40 Ma from ~5 to ~15 cm/yr (Pardo-Casas and Molnar, 1987), then decreased to ~6 cm/yr around 40 Ma and remained low (4–6 cm/yr) until ~35 Ma. From ~35 to ~25 Ma convergence rate

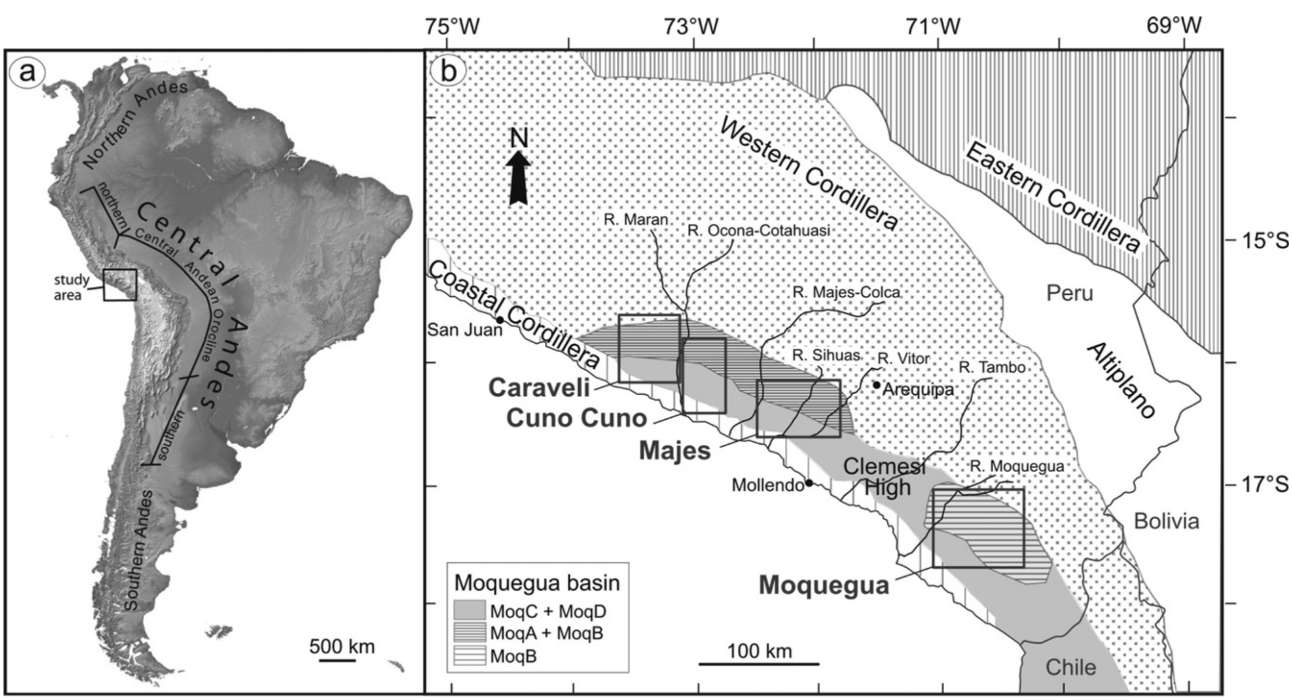

Fig. 1. a) Location of the study area in southern Peru within the Andean Cordillera (modified after Sempere et al., 2002). b) Simplified geomorphological map of the Central Andean Orocline in Southern Peru (study area), modified after Decou et al. (2011). Grey boxes show the four studied sections. The MoqA + MoqB areas are mostly overlain by MoqC + MoqD sediments.

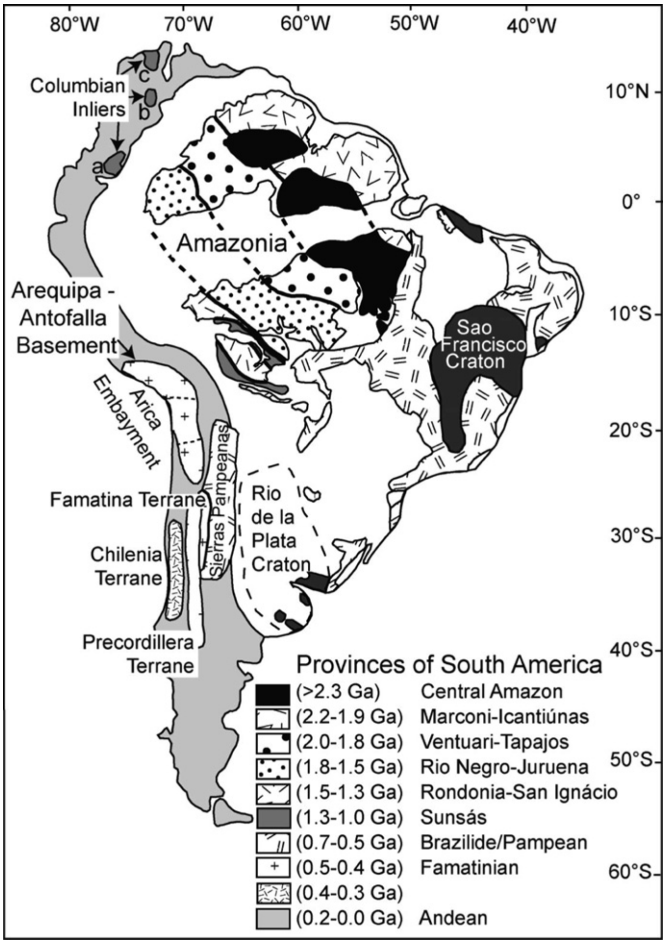

Fig. 2. Map of the main age provinces composing the South American continent after Cordani et al. (2000) and Tassinari et al. (2000).

gradually increased to reach again ~15 cm/yr. Since ~20 Ma till the present day a progressive decrease to ~8 cm/yr has been shown by Somoza (1998).

In the study area, the Paleozoic to Cenozoic sedimentary and volcanic rocks of the western margin of Gondwana are underlain by two major accreted terrains: the Arequipa Massif and the Amazonian Craton. The Arequipa Massif is a single metamorphic Proterozoic crustal block exposed along the Central Andean western margin and comprises two age domains which are slightly younger in the north (1819 + 17/−16 Ma; San Juan) than in the south (1851 ± 5 Ma; Mollendo) (Shackleton et al., 1979; Loewy et al., 2004). The Amazonian Craton is exposed to the east of the present Eastern Cordillera and is divided into two Archean nuclei (>2.3 Ga) and five tectonic provinces: Marconi-Icantiúnas (2.2–1.9 Ga), Ventuari-Tapajos (2.0–1.8 Ga), Rio Negro Juruena (1.8–1.5 Ga), Rondonia-San Ignácio (1.5–1.3 Ga) and Sunsás/Grenvillian event (1.3–0.95 Ga) (Fig. 2). Those provinces were formed prior to the Neoproterozoic through accretion events (Tassinari et al., 2000; Cordani et al., 2009). The accretion of the Arequipa Massif to the Amazonian Craton occurred during the Sunsás orogeny (1.20–0.94 Ga). Those two units were both later affected by the Pampean/Braziliano orogeny (0.7–0.5 Ga) (Forsythe et al., 1993; Loewy et al., 2004). Moreover, the entire Arequipa Massif has been affected by the Famatinian (0.5–0.4 Ga) continental arc (Casquet et al., 2001; Loewy et al., 2004; Chew et al., 2007; Bahlburg et al., 2009; Otamendi et al., 2009) and thus records mainly late Paleoproterozoic (1.9–1.7 Ga) and Famatinian ages (Loewy et al., 2004).

The metamorphic basement is covered by Paleozoic sediments (Bahlburg and Hervé, 1997; Wörner et al., 2000b) which are in turn overlain by Mesozoic back-arc strata of the Arequipa–Tarapaca basin (Vicente, 2005, 2006) (Fig. 3). Locally the Mesozoic sedimentary fill of the Arequipa–Tarapaca basin is referred to as Yura (Peru) or Livilcar (Chile) formations for the quartzarenite-rich units and referred to as Chocolate Formation for the volcanic/volcaniclastic deposits reflecting the activity of the Late Triassic to Early Jurassic Chocolate arc (Vincente et al., 1982; Acosta et al., 2010). The back-arc strata are frequently intruded by plutonic rocks of the Late Cretaceous to Early Eocene Toquepala arc (Mamani et al., 2010) which represent the latest phase of the Coastal Batholith. The main intrusive phases of the Coastal Batholith, in southern Peru, include the Late Liassic (~190–180 Ma), the Middle to Late Jurassic (~165–150 Ma), the late Early Cretaceous (~115–100 Ma) and, finally, the Late Cretaceous to Eocene interval (~91–45 Ma) (Mukasa, 1986; Clark et al., 1990; Mamani et al., 2010). In the Central Depression of the southern Peruvian forearc, between the Coastal Cordillera and the Western Cordillera, all these strata are overlain by Cenozoic sediments referred to as the Moquegua Group (Roperch et al., 2006) which has its equivalents in northernmost Chile (Azapa, Oxaya and Diablo formations, Fig. 3; Wörner et al., 2000a; Pinto et al., 2007). In the following we give a brief description of the geology and stratigraphy of the Paleozoic and Mesozoic sedimentary basins (as potential source rocks of the Moquegua clastic sediments), followed by the Cenozoic basins being the main target of this study.

2.1. Ordovician to Devonian basins

The Ordovician to Devonian sedimentary basins (Fig. 3) in Southern Peru are bound to the east by the Amazonian Craton and to the west by the Arequipa Massif. The Ordovician basins were most likely formed in an active plate margin setting (Loewy et al., 2004; Bahlburg et al., 2006; Chew et al., 2007; Miskovic and Schaltegger, 2009; Miskovic et al., 2009) that persisted until early Devonian, when it probably evolved into a passive margin (Bahlburg and Hervé, 1997; Cawood, 2005). The sedimentary rocks of the Ordovician basins are presently exposed in the Eastern Cordillera and Altiplano whereas the Devonian sediments only outcrop on the Altiplano and in the Majes Valley (near Aplao). Generally Ordovician to Devonian sedimentary strata evolve from deep to shallow marine turbiditic sandstones and shales (Reimann et al., 2010). About 3000 m of Paleozoic sedimentary rocks are overlying the Amazonian Craton at its eastern margin and the Arequipa Massif on its western part.

2.2. Mesozoic basin (Yura Group)

The Arequipa–Tarapaca basin (Vicente, 1981) has been deposited during the Ordovician to Devonian (Fig. 3). The Mesozoic sedimentary basin formed by back-arc rifting during Jurassic to early Cretaceous time (Vicente et al., 1982; Vicente, 2006). Located northwest of Arequipa, the most complete sequence of the Yura Group sedimentary rocks has been described by Wilson and García (1962) and Vicente (1981). This sequence measures more than 2000 m in thickness and is divided, from bottom to top, into five formations: Chocolate, Socosani, Puente, Cachíos and Labra (Sempere et al., 2002). The Late Triassic–Early Jurassic Chocolate formation is dominated by volcanic and volcaniclastic material and is unconformably overlain by shallow marine carbonates of the late Liassic Socosani Formation followed by the turbidite succession of the Puente Formation (Acosta et al., 2011; Vicente et al., 1982; Vicente, 1989). The Cachíos Formation mostly consists of organic-rich shale and grades to the sandstone-dominated Labra Formation (Vicente

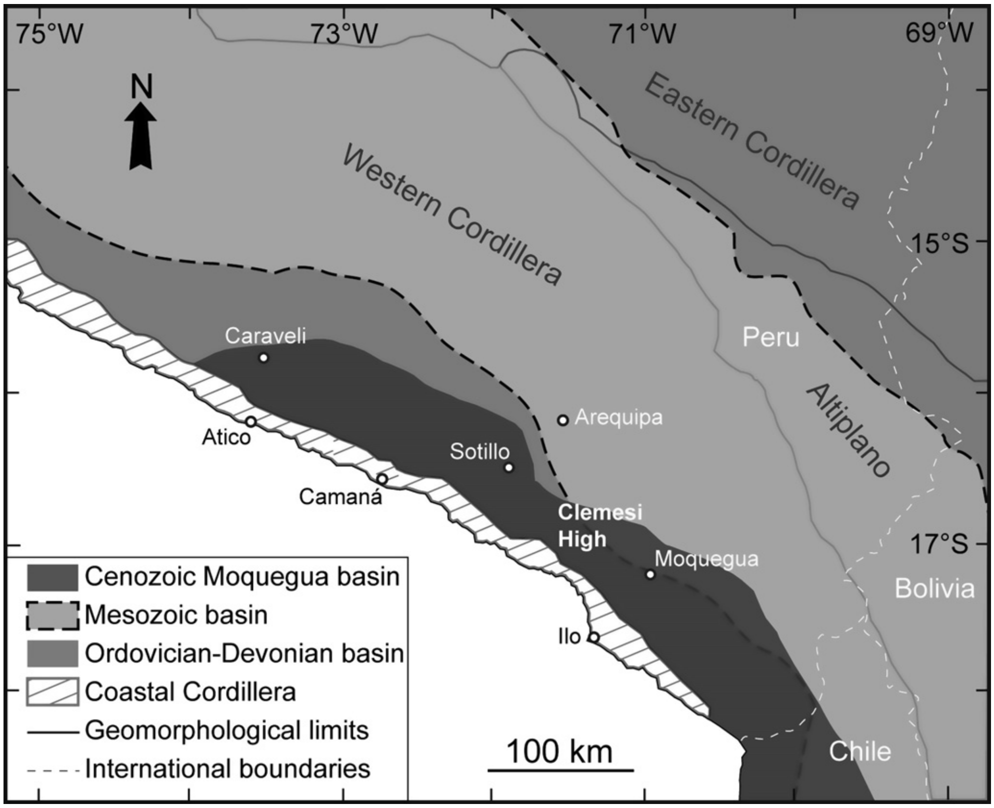

Fig. 3. Map of the three main sedimentary basins of the area using information from INGEMMET and Reimann et al. (2010). The boundaries of geomorphological units refer to Fig. 1b.

et al., 1982; Sempere et al., 2002). From the early Late Jurassic (~160 Ma) until ~130 Ma hundreds of meter of quartzarenites were accumulated (Labra Fm., Upper Yura Group). These quartzarenites constitute the main provenance-relevant unit of the Yura Group and can be found frequently as pebbles in the Cenozoic deposits and thus have to be considered as an important source for detrital zircon. The southernmost outcrops of the Mesozoic sedimentary basin can be found across the Chilean border, at least as far as Guatacondo valley (21°S; Wotzlaw et al., 2011).

2.3. Cenozoic forearc basins (Moquegua Group)

The Moquegua sedimentary basin (Fig. 3) is bounded by the Coastal Cordillera to the southwest and the Western Cordillera to the northeast. Towards the southwest, thinning-out onlap geometries as well as the distribution of continental facies suggest that the Moquegua basin was apparently bounded by the Coastal Cordillera during much of its activity, with only a couple of fluvial outlets reaching the Pacific Ocean from the Early Miocene on (Sempere et al., 2004; Roperch et al., 2006). The Moquegua Group is divided into four units and was deposited between ~50 and ~4 Ma (MoqA, MoqB, MoqC and MoqD; Roperch et al., 2006).

The MoqA and lower MoqB units (Fig. 1b) were deposited in endorheic basins, the center of which were occupied by mudflat to lacustrine or playa-lake environments, toward which a few low-energy river systems converged (Decou et al., 2011). In contrast, the coarser MoqC and MoqD units (Fig. 1b) accumulated in higher energy alluvial environments and are characterized by a marked volcanic contribution. An overall coarsening upward is already observed for middle and upper parts of MoqB, especially in Caraveli, Majes and Moquegua sections (Decou et al., 2011). MoqC is subdivided in a lower unit (C1) with generally fine-grained sediments and still low amounts of volcanic material similar to middle/upper MoqB deposits. However, the sediment grain size for MoqC1 varies between localities. Coarser sediments are observed in the Cuno Cuno section while finer MoqC1 sediments are common in Majes and Moquegua sections. The upper unit (C2), which is mainly composed of coarse-grained sediments, shows high abundances of volcanic material (Decou et al., 2011).

A recently revised chronostratigraphic framework (Decou et al., 2011) suggests that the MoqA unit was deposited between ~50 Ma and ~40 Ma, the MoqB unit between ~40 Ma and 30 Ma, the MoqC unit between 30 Ma and ~15–10 Ma and the MoqD unit between ~15 and 10 Ma and ~4 Ma approximately, possibly with local variations (Sempere et al., 2004; Roperch et al., 2006; Decou et al., 2011). The C1 to C2 boundary was tentatively placed at ~25 Ma in agreement with the onset of major ignimbrite forming volcanism in the area. A key observation is that MoqA and MoqB units were deposited in two distinct sub-basins that are separated by the Clemesí High (Fig. 1b). In contrast, MoqC and MoqD units accumulated in one single, large depositional domain (Fig. 1b) stretching along the foot of the present-day Western Cordillera (Roperch et al., 2006). In the northwestern sub-basin, the MoqA unit mainly overlies (1) intrusive rocks belonging to the Coastal Batholith, (2) tilted, quartzarenite-rich strata of the Mesozoic Yura Group in the Majes valley, and (3) the Arequipa Massif metamorphic basement and minor Paleozoic outcrops along its southern rim (Cuno Cuno section; southern Majes valley). In contrast sedimentation in the southeastern sub-basin starts with the MoqB unit as MoqA was not deposited. In the entire southeastern sub-basin (which includes the Moquegua section), the Moquegua Group overlies the Toquepala Group, a >1.5 km-thick pile of volcanic rocks that accumulated in an arc setting between ~91 and 45 Ma (Mamani et al., 2010).

3. Samples and methods

We sampled sandstones from the four stratigraphic units of the Moquegua Group (MoqA, MoqB, MoqC and MoqD) along four sections (from NW to SE: Caravelí, Cuno Cuno, Majes and Moquegua) (Fig. 1b, Table 1). In addition we collected the potential source rocks of the Moquegua sediments, mainly in the form of pebble populations (Dunkl et al., 2009). Gneisses from the Proterozoic Arequipa Massif and quartzarenite from Late Jurassic to Early Cretaceous Yura Group were also taken from outcrops. Permian to Early Cretaceous arc rocks, which mainly crop out in the Coastal Cordillera (e.g. Chocolate Formation), were not considered as potential source for Moquegua basin sediments since their contribution would have been restricted to the south western distal edge of the basin.

After crushing and sieving, heavy minerals were separated from the 63–125 μm fraction by sodium-polytungstate, followed by magnetic separation to concentrate zircons. For each sample (source and sediment) one part of the zircons was embedded in PFA teflon for fission track dating. From the second fraction, zircon crystals were hand-picked, under a binocular microscope, and embedded in epoxy for U–Pb dating. Crystal mounts were polished using diamond suspensions to expose the internal parts of the grains.

For U–Pb dating, cathodoluminescence (CL) images of each polished zircon crystal were taken using the JEOL JXA 8900 electron microprobe at the Geosciences Center of Göttingen University. The microprobe was set to an accelerator voltage of 20 kV and a beam current of 15 nA. U and Pb isotope ratio measurements were performed at the Geological Survey of Denmark and Greenland in Copenhagen (Denmark) using a ThermoFinnigan Element2 double focusing magnetic sector field inductively coupled plasma mass spectrometer (SF-ICP-MS) according to the method described by Frei and Gerdes (2009). The SF-ICP-MS is coupled to a New Wave UP-213 laser ablation system. Sample ablation spots were preset with blocks of 10 unknowns bracketed by blocks of 3 zircon standards (GJ-1) (Jackson et al., 2004). Ablation was performed in single spot mode with a spot diameter of 30 μm. The laser was set at a frequency of 10 Hz with a nominal energy output of 50%. Background signal intensity was measured for 30 s prior to 30 s dwell time and followed by at least 20 s of washout time. The U–Pb ages were calculated using PepiAGE software (Dunkl et al., 2008). Probability density plots were made with AgeDisplay (Sircombe, 2004).

For fission track (FT) analysis, the spontaneous tracks were revealed by etching technique using an eutectic melt of NaOH–KOH at 225 °C (Gleadow et al., 1976). Etching time varied from 25 to 106 h. Neutron irradiations were performed at the research reactor of Technical University of Munich in Garching (Germany). We used low-uranium muscovite sheets (Goodfellow mica) as external detector (Gleadow, 1981). After irradiation the induced fission tracks in the mica detector were revealed by etching in 40% HF for 30 min. Track counts were made with a Zeiss-Axioskop microscope equipped with a computer-controlled stage system (Dumitru, 1993) at the Geosciences Center of Göttingen University, at magnification of 1000. The FT ages were determined by the zeta method (Hurford and Green, 1983) using age standards listed in Hurford (1998). The error of the FT age was calculated using the classical procedure, i.e., by Poisson uncertainty of the track counts (Green, 1981). Calculations and plots were made with TRACKKEY program (Dunkl, 2002). The dominant age clusters were identified by PopShare software assuming Gaussian distribution for the individual age clusters and the goodness of fit was tested by the RMS method (Dunkl and Székely, 2002).

4. Results and interpretations

4.1. U–Pb data

4.1.1. Source rocks

The Proterozoic Arequipa Massif metamorphic basement has a specific zircon U–Pb age distribution that is characterized by a dominant 1.1 Ga age cluster (Fig. 4a, b; see also Loewy et al., 2004; Bahlburg et al., 2009; Casquet et al., 2010). However, in some areas

Table 1
Description of the samples (potential sources and sediments) used for this study.

Sample	Formation	Section	Lithology	Type	UTM Easting	UTM Northing	Elevation (m a.s.l.)	Zircon U–Pb dating	Zircon fission track dating
MAJ-04-241	Meso. basement	Majes	Quartzarenite	Outcrop	0770926	8209328	506		X
YUR-08-01	Meso. basement	Majes	Quartzarenite	Outcrop	0201156	8201688	2350		X
YUR-08-03	Meso. basement	Majes	Quartzarenite	Outcrop	0197550	8207608	2522	X	X
MAJ-10-01	In MoqA unit	Majes	Quartzarenite	Pebbles	0769668	8220142	616		X
LOC-08-04	In MoqB unit	Moquegua	Quartzarenite	Pebbles	0323313	8057498	775	X	X
MAJ-08-03	In MoqB unit	Majes	Quartzarenite	Pebbles	0770884	8217557	664	X	X
CUC-08-02	In MoqC (C1) unit	Cuno Cuno	Quartzarenite	Pebbles	0704039	8231034	1792		X
LOC-08-01	In MoqC (C2) unit	Moquegua	Quartzarenite	Pebbles	0339623	8073425	1363		X
VIT-10-01	In MoqD unit	Majes	Quartzarenite	Pebbles	0184537	8178089	1383		X
MAJ-07-12	In river bed	Majes	Quartzarenite	Pebbles	0769833	8221064	618	X	X
OCO-08-03	In river bed	Cuno Cuno	Quartzarenite	Pebbles	0701241	8184144	26	X	X
COL-07-19	In river bed	Majes	Quartzarenite	Pebbles	0235567	8287749	3835	X	X
OCO-07-33	In river bed	Cuno Cuno	Quartzarenite	Pebbles	0705274	8252909	639		X
MAJ-07-03	In MoqD unit	Majes	Gneiss	Pebbles	0769967	8188148	1034	X	X
OCO-07-03	In river bed	Cuno Cuno	Gneiss	Pebbles	0701460	8277627	925	X	X
OCO-08-04	In river bed	Cuno Cuno	Gneiss	Pebbles	0701241	8184144	26		X
MAJ-07-04	MoqD	Majes	Sandstone		0770085	8188325	1035	X	X
MOQ-10-02	MoqD	Moquegua	Sandstone		0273223	8089602	1229	X	X
CUC-08-04	MoqC (C2)	Cuno Cuno	Sandstone		0704833	8230329	1991	X	X
MAJ-07-40	MoqC (C2)	Majes	Sandstone		0771263	8191925	859	X	X
MOQ-04-218	MoqC (C2)	Moquegua	Sandstone		0295148	8091684	1749		X
CUC-05-01	MoqC (C1)	Cuno Cuno	Sandstone		0704018	8230855	1792	X	X
MAJ-10-02	MoqB	Majes	Sandstone		0770999	8211503	519	X	X
LOC-05-04	MoqB	Moquegua	Sandstone		0323627	8057419	776	X	X
MOQ-08-02	Base MoqB	Moquegua	Sandstone		0285985	8079622	938		X
CARA-10-02	MoqA	Caraveli	Sandstone		0673518	8249243	1941	X	X
MAJ-07-13	Base MoqA	Majes	Sandstone		0770769	8216251	709	X	X

of the Eastern Cordillera and Altiplano, the Arequipa Massif records ages of a younger metamorphic overprint between 473 and 440 Ma (Wörner et al., 2000b; Loewy et al., 2004; Bahlburg et al., 2006, 2009) corresponding to the Famatinian event. The two subordinate peaks around 1.8 and 1.5 Ga (Fig. 4b) have to be taken with caution due to of the low number of dated zircon from this sample.

As presented in Reimann et al. (2010) Ordovician sediments from the Eastern Cordillera and Altiplano (Fig. 4c, d) show a major provenance from the Amazonian Craton and Brazilian shield with a very strong contribution from the Arequipa Massif for Ordovician sediments from the Altiplano. Devonian sediments from the Altiplano (Fig. 4) have a provenance from the Brazilian shield (Reimann

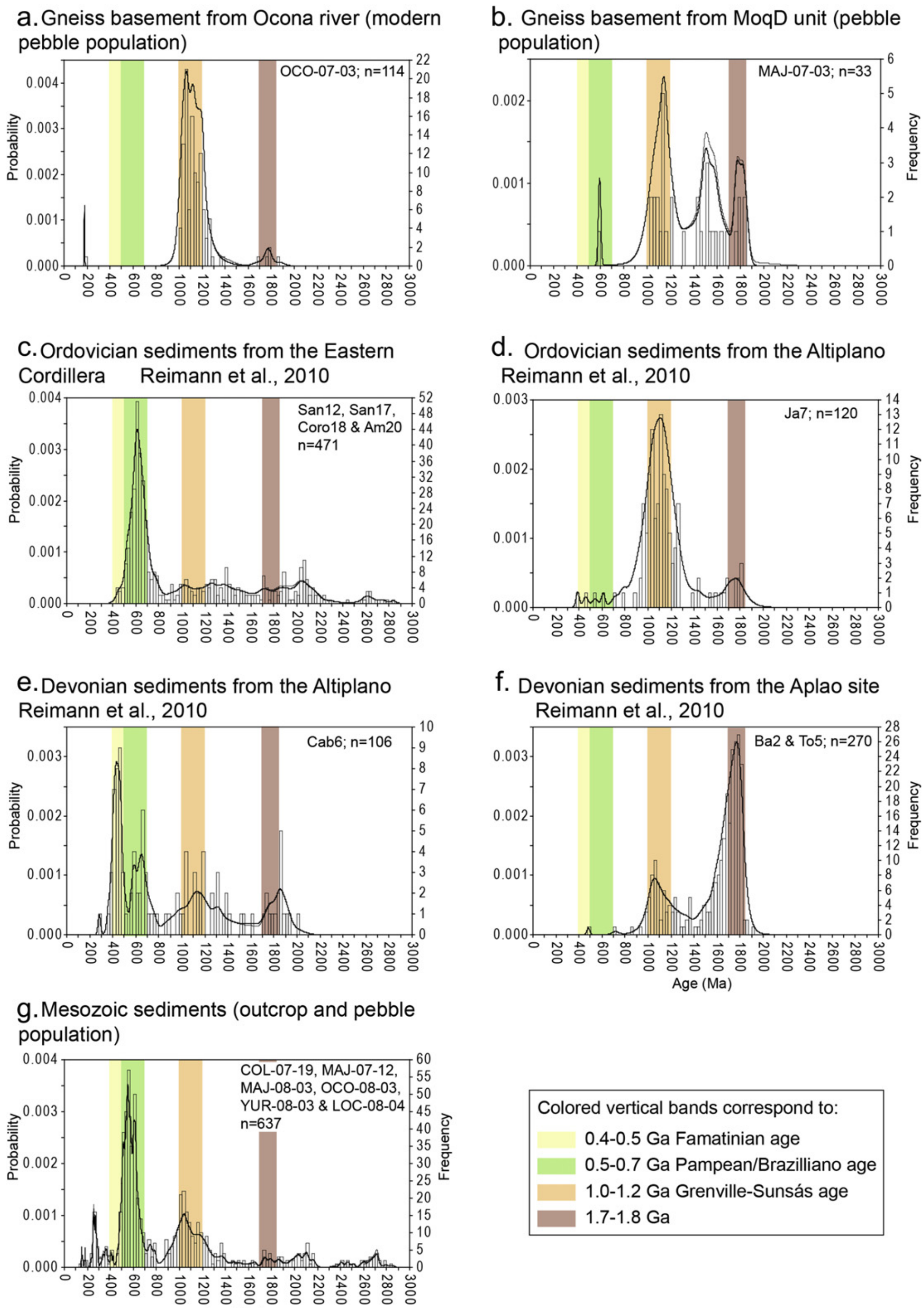

Fig. 4. Zircon U–Pb ages distribution for the potential source rocks. a–b: Arequipa Massif gneisses, c–f: Ordovician–Devonian basin sediments (after Reimann et al. (2010)), g: Mesozoic basin sediments. Probability (left axis) and frequency (right axis) are plotted versus age for each diagram. Ages <800 = $^{238}U/^{206}Pb$ ages; ages >800 = $^{207}Pb/^{206}Pb$ ages (Nemchin and Cawood, 2005; Kolodner et al., 2006). All grains with a concordance between 90 and 110% are plotted.

et al., 2010) and a strong input from the Arequipa Massif. In addition we note a distinct presence of Famatinian ages in the Devonian sediments from the Altiplano, whereas the Devonian sediments from Aplao site (Fig. 4f) have an exclusive provenance from the Arequipa Massif (Reimann et al., 2010). Zircon grains older than 2.5 Ga are essentially derived from the Archean Craton (Casquet et al., 2010) but are assumed to have been recycled from Ordovician and/or Mesozoic strata into the Cenozoic Moquegua Basin sediments.

Zircon U–Pb ages from six Mesozoic quartzarenite samples both from outcrops and pebble populations (Fig. 4g) show major age clusters between 700 and 500 Ma and 1.2–1.0 Ga, with minor peaks between 100 and 400 Ma. The 100–400 Ma peak largely coincides with the Late Triassic to Early Jurassic Chocolate volcanic arc activity (Mamani et al., 2010), whereas the other two main age clusters reflect the Pampean–Braziliano (700–500 Ma) and Grenville–Sunsás (1.2–1.0 Ga) orogenic cycles. From all well characterized potential source rocks from the Eastern Cordillera and Altiplano (Reimann et al., 2010), Ordovician sediments from the Eastern Cordillera (Fig. 4c) are the only potential source with a redominant Pampean–Braziliano age pattern. Due to missing Famatinian (500–400 Ma) ages in the Mesozoic sediments, the Devonian sediments from the Altiplano (Fig. 4e) are not considered as a significant source. Similarly, the low number of zircon ages between 1700 and 1850 Ma preclude Devonian rocks like those exposed at Aplao (Fig. 4f). The Grenville–Sunsás age peak most likely derives from recycling of Ordovician sediments from the Altiplano (Fig. 4d) and/or erosion of gneisses from the Arequipa Massif (Fig. 4a, b). Zircon grains with an age between 100 and 400 Ma most likely derived from the Permian to Jurassic Chocolate arc.

4.1.2. Moquegua sandstones

Zircon ages from base MoqA sediments from Majes section (Fig. 5g) range from 50 Ma to 2 Ga and cluster at Grenville–Sunsás ages (1.2–1.0 Ga) and around 1.9–1.7 Ga. These two clusters indicate a predominantly local source Devonian sediments from the Aplao region (Fig. 4f; Reimann et al., 2010) with a likely contribution from Ordovician sediments from the Altiplano (Fig. 4d). An additional potential source could be Arequipa Massif gneisses which are locally available, but these would have to be unaffected by Famatinian metamorphism (Fig. 4a, b). Pampean–Braziliano ages, which are predominant in the Mesozoic sediments (Fig. 4g), are largely missing (only 3 grains out of 113) in MoqA sandstones from Majes. This indicates that the Mesozoic sediments cannot be considered as important source rock for the base of MoqA in Majes Valley although MoqA locally overlies the Mesozoic strata.

At Caravelí, zircon ages from MoqA sandstones (Fig. 5h) are different compared to Majes. A prominent Famatinian (500–400 Ma) age cluster suggests strong contribution from Devonian sediments from the Altiplano (Fig. 4e) and/or the Arequipa Massif with Famatinian overprint (Loewy et al., 2004; Chew et al., 2007; Bahlburg et al., 2009). Given the absence of Famatinian ages in the gneiss pebble population from nearby Ocoña river (Fig. 4a), we argue for a strong contribution from the Altiplano. Due to the abundance of Grenville–Sunsás (1.2–1.0 Ga) ages and a minor cluster around 1.9–1.7 Ga, however, significant contribution from Arequipa Massif gneisses (Fig. 4a, b) is most likely. Minor input from Ordovician sediments of the Altiplano (Fig. 4d) cannot be excluded. The five zircon grains dated between 100 and 200 Ma (Fig. 5h) most likely derived directly from the Jurassic Chocolate volcanic arc. Recycling from the Mesozoic sedimentary rocks (Fig. 4g) is considered minor, like in Majes (see above) due to the almost complete absence of Pampean–Braziliano ages.

Zircon ages from top MoqB sediments from the Majes area (Fig. 5e) cluster at Pampean–Braziliano (700–500 Ma; plus few Famatinian grains) and Grenville–Sunsás (1.2–1.0 Ga) ages, as well around 1.9–1.7 Ga. These three clusters highlight a major provenance from Mesozoic sediments (Fig. 4g) with likely contributions from Arequipa Massif gneisses (Fig. 4a, b) and Devonian sediments from Aplao (Fig. 4f). Moreover, sandstones from top MoqB show the first occurrence of zircons younger than 100 Ma (9 out of 108) ranging from 70 to 100 Ma (Fig. 5f). Such ages indicate a direct provenance from the Toquepala arc (91–45 Ma) whereas ages between 90 and 100 Ma and several Triassic to Lower Cretaceous grains resemble typical Chocolate arc ages that likely derive from recycling of Mesozoic sediments (Fig. 4g).

Zircon ages from base MoqC (C1) sediments (approx. 30–25 Ma) from the Cuno Cuno section (Fig. 5c) show three age clusters: the Pampean–Braziliano (700–500 Ma) and Grenville–Sunsás (1.2–1.0 Ga) cluster, similar to the top MoqB sample from Majes (Fig. 5e), and a third one between 25 and 40 Ma (Fig. 5d). The two older clusters represent a major contribution from the Mesozoic sediments (Fig. 4g) whereas the youngest cluster (~25% of measured zircons) indicates a significant contribution from the Andahuaylas–Anta volcanic arc (45–30 Ma; Mamani et al., 2010). Only one single grain may derive from the Toquepala arc (Fig. 5d).

For the ~25 to ~15 Ma MoqC (C2) sediments (Fig. 5b) the majority of zircon grains fall into a narrow and largely synsedimentary age range between 20 and 30 Ma. This cluster emphasizes a major provenance from the 30–24 Ma Tacaza arc and for ages younger than 24 Ma a contribution from the 24–10 Ma Huaylillas arc is feasible. A minor contribution (4 grains) probably represent the 91–45 Ma Toquepala arc. Beyond the predominant young magmatic sources, a significant contribution from the Mesozoic sediments is obvious (30 grains out of 127 are older than 100 Ma). For MoqD sediments (Fig. 5a) ~90% of the zircon ages are <100 Ma and ~75% cluster at 10–5 Ma. This implies that the dominant source for the MoqD sediments is the 10–3 Ma Lower Barroso volcanic arc with minor additional input from the 24–10 Ma Huaylillas, 30–24 Ma Tacaza and 45–30 Ma Andahuaylas–Anta arcs. A minor contribution from Mesozoic sediments is also observed (14 grains out of 128 are older than 100 Ma and interpreted to be derived from Mesozoic sediments), and confirmed by the presence of mature quartzarenite pebbles in MoqD conglomerates.

4.2. Zircon fission track data

4.2.1. Source rocks

Zircons from the Proterozoic Arequipa Massif gneisses are mainly pink-coloured and rounded or angular in shape. Zircon fission track (ZFT) data for the Arequipa Massif consistently indicate Late Cretaceous to Early Paleogene cooling (Fig. 7a–c). The presence of grains with Paleozoic and Early Mesozoic ages, especially in the modern Ocoña river sample (Fig. 7c), suggests that not all fission track ages in the Arequipa Massif have been completely reset. The timing of the thermal overprint coincides with Toquepala age volcanic arc activity (91–45 Ma) and late stages of the Chocolate arc (i.e. late Early Cretaceous phase of Coastal Batholith plutonism; see above).

ZFT data obtained from the late Jurassic to Early Cretaceous quartzarenites (Fig. 6a–g) show three major age clusters: Triassic, Jurassic and Eocene (Table 2). The zircons from the Mesozoic quartzarenite are transparent and mostly rounded. The Triassic age cluster is observed in both, the quartzarenites pebble population samples and outcrop samples from Majes valley (Fig. 6a). The Jurassic age cluster, however, is present in the modern quartzarenite pebble population from Ocoña river and also in outcrop samples from Yura (Yura Group) (Fig. 6b). These two age clusters correspond in time to the voluminous volcanic arc products of 310–91 Ma Chocolate Formation. Moreover, grains of Triassic to Jurassic ages were also

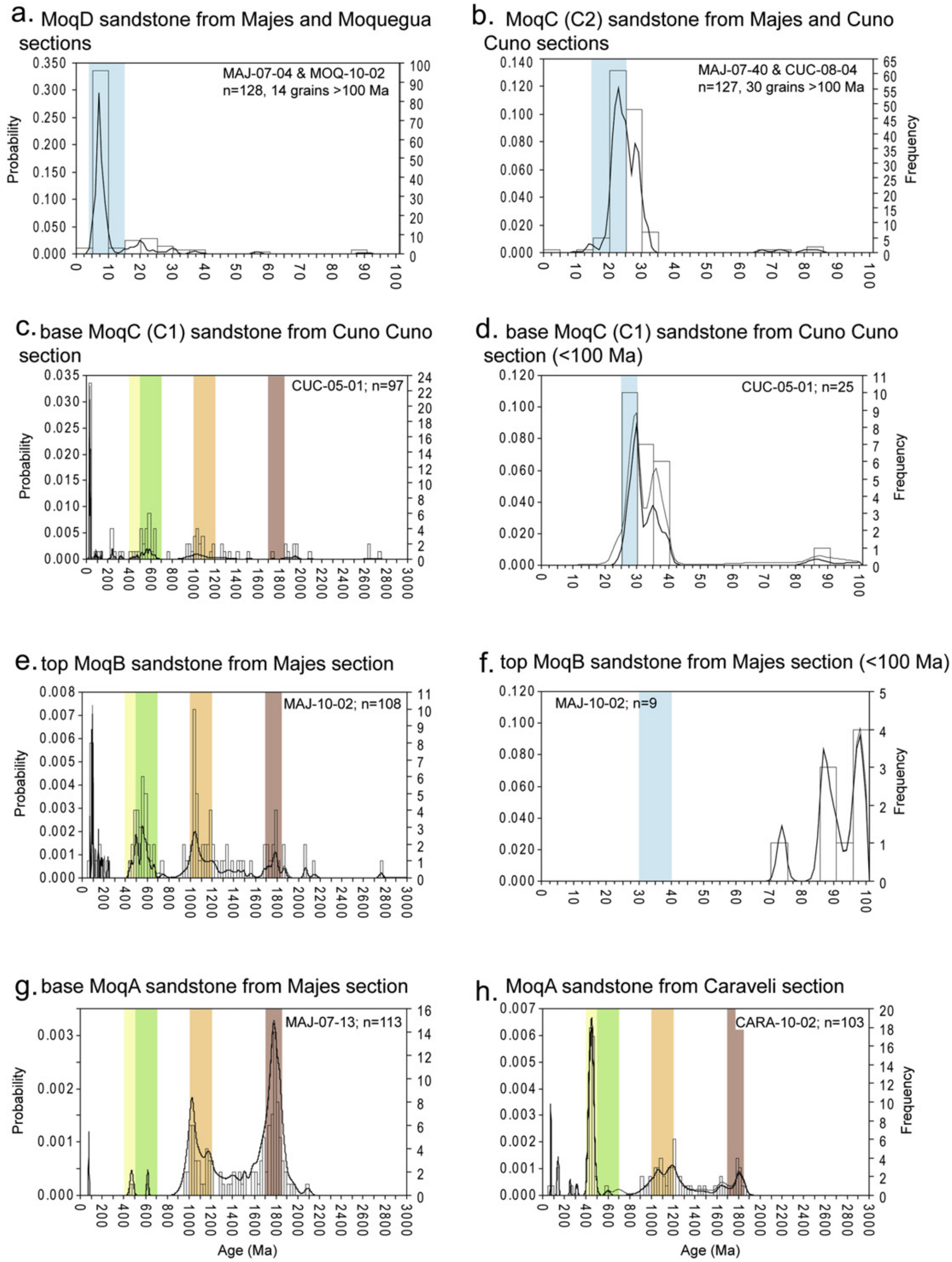

Fig. 5. Zircon U–Pb ages distribution for the Moquegua Group sediments. a. sediments from MoqD unit, b. sediments from MoqC2 unit, c–d. sediments from MoqC1 unit, e–f. sediments from MoqB unit and g–h. sediments from MoqA unit. Probability (left axis) and frequency (right axis) are plotted versus age for each diagram. Ages <800 = $^{238}U/^{206}Pb$ ages; ages>800 = $^{207}Pb/^{206}Pb$ ages (Nemchin and Cawood, 2005; Kolodner et al., 2006). Sedimentation ages are indicated by a blue bar on the zoomed diagrams only (ages <100 Ma in a, b, d, f). For key see Fig. 4. (For interpretation of the references to colour in this figure legend, the reader is referred to the web version of this article.)

detected using U–Pb dating method (Fig. 4g), suggesting that some ZFT data reflect formation ages and are thus most likely derived directly from Chocolate arc volcanic that formed at this time. The Paleogene cluster is largely represented in pebble populations from Moquegua Group B and C2 units (see below and Fig. 6d, e) and is best explained by partial or total thermal reset of the fission track ages in the Mesozoic sedimentary rocks due to the activity of the 91–45 Ma Toquepala volcanic arc.

ZFT data from Mesozoic quartzarenite pebble populations sampled along the Moquegua Group sequence from MoqA to MoqD result in strikingly different age distributions (Fig. 6c–g). The quartzarenite pebble population sampled from MoqA conglomerates at Majes (Fig. 6g) has a broad Permo-Mesozoic age cluster (∼300–150 Ma) and the pebble population from MoqC1 unit at Cuno Cuno (Fig. 6f) has a slightly younger Triassic–Jurassic age cluster (∼225–125 Ma). Both samples show only few Cenozoic

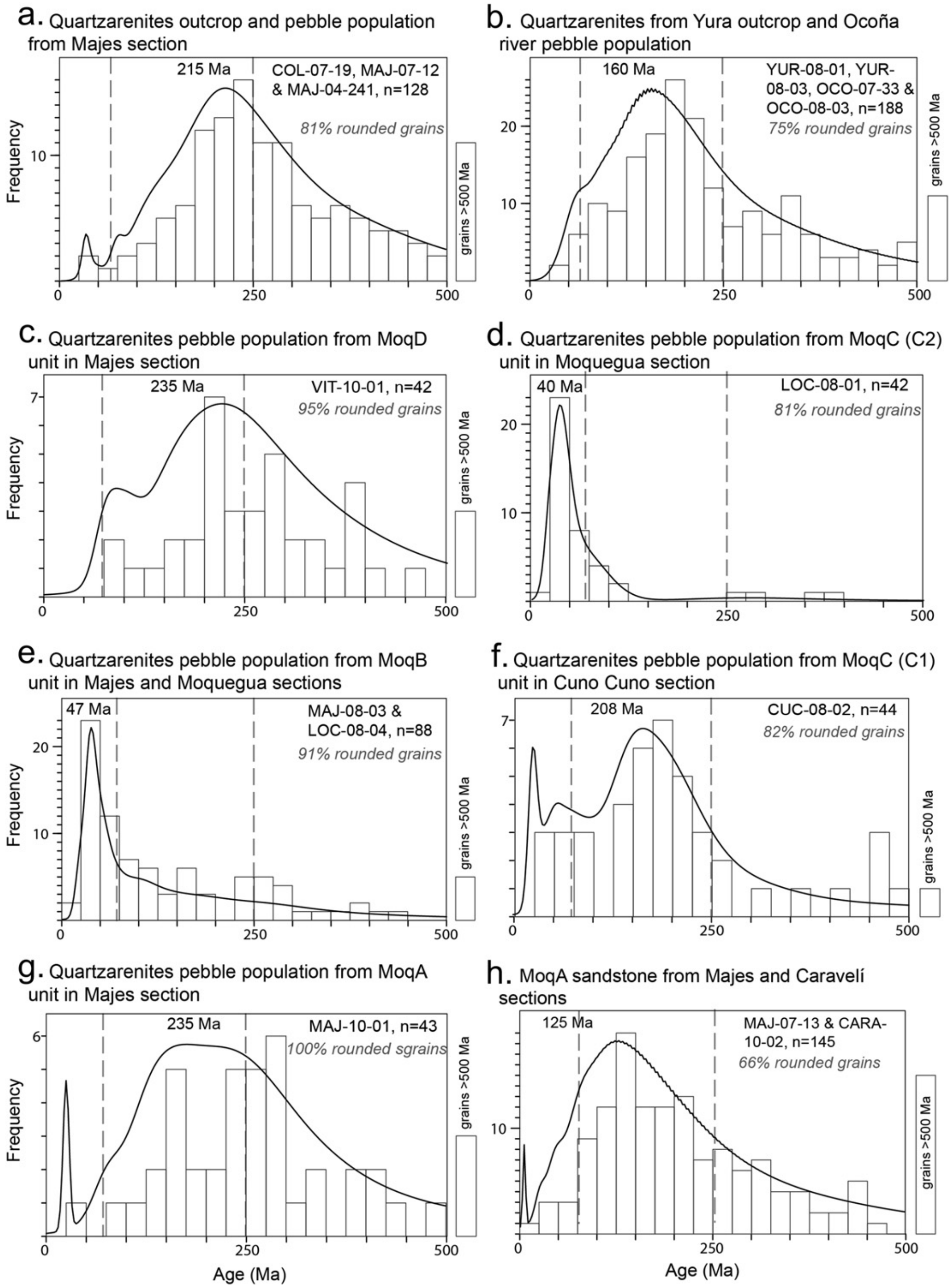

Fig. 6. Zircon fission track single grain age distributions for the Mesozoic quartzarenites and Moquegua Group samples. a–b. quartzarenite samples from outcrop and modern river, c–g. quartzarenite pebble populations from the Moquegua Group stratigraphic units and h. sandstone samples from MoqA unit. Probability density curves are calculated according to Hurford et al. (1984).

ages (~5%). These patterns are broadly similar to present-day outcrop and modern pebble population data (Fig. 6a–b) indicating a provenance of thermally non-reset Mesozoic sediments during MoqA and MoqC1 (in Cuno Cuno) deposition. From the MoqB unit (Fig. 6e), quartzarenite pebble population samples contain Mesozoic ZFT ages and a significant proportion of zircons with Tertiary cooling ages that peak in the Eocene (~28%). This suggests provenance from Mesozoic sediments that partly experienced reset of ZFT chronometer in Eocene. The quartzarenite pebble population from MoqC2 unit at Locumba Valley (Moquegua section) (Fig. 6d) has a dominant Eocene age cluster (~77%) and only very few grains showing Mesozoic age. This age population implies a provenance from Mesozoic sediments that were largely reset in Paleocene to Eocene time. In strong contrast, quartzarenite pebble population from MoqD unit (Fig. 6c) at Vitor valley (Majes section) shows very similar age distribution to those observed for

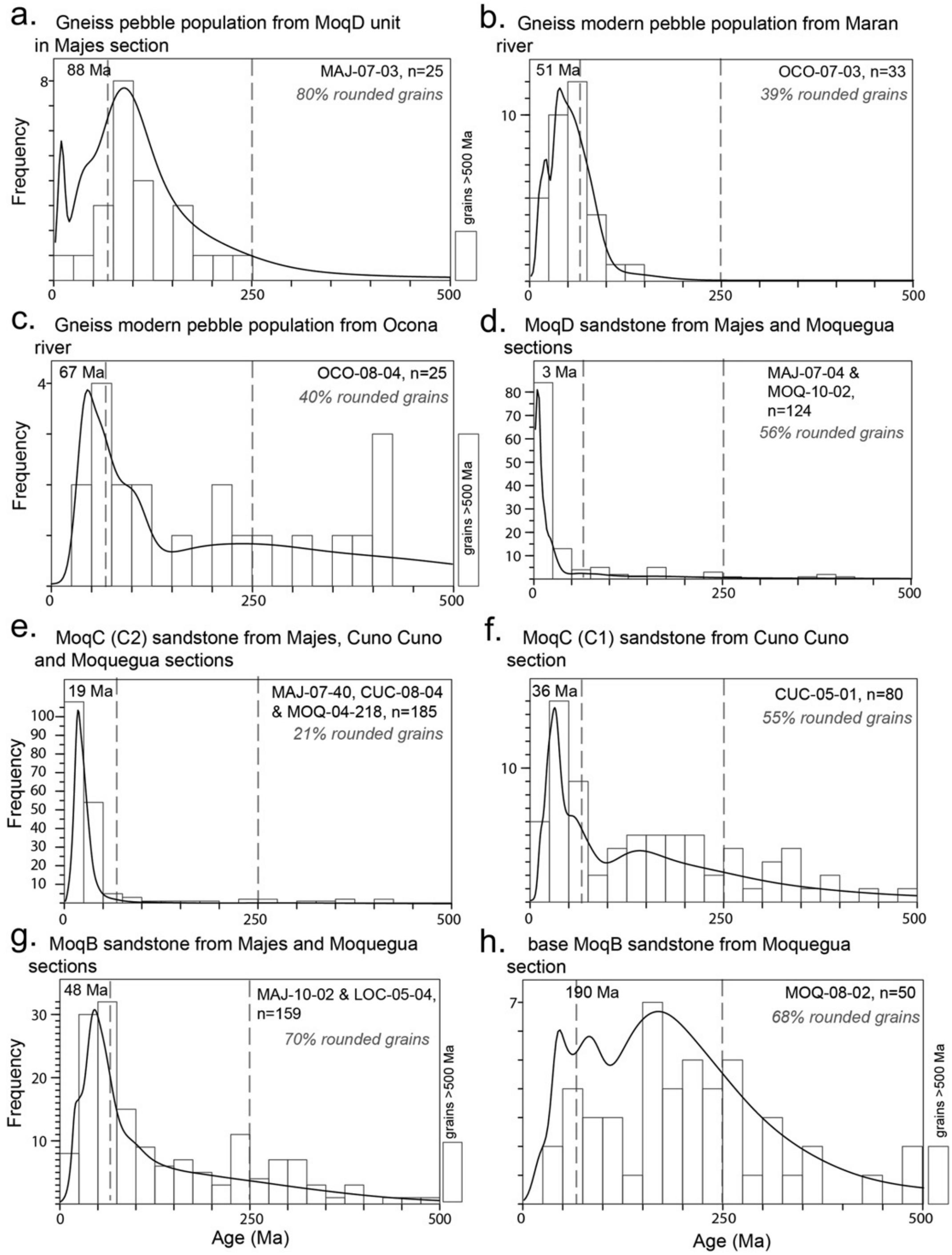

Fig. 7. Zircon fission track single grain age distributions for the Arequipa Massif gneisses basement (a–c) and the Moquegua Group sediments (d–h). Frequency is plotted versus age for each diagram.

MoqA (Fig. 6g) and modern pebble populations and outcrop data (Fig. 6a, b). This implies provenance from thermally non-reset Mesozoic sediments and/or recycling from the MoqA unit. Clearly, recycling of quartzarenite pebbles from older MoqB and MoqC2 conglomerates cannot explain the observed ZFT distributions in MoqD and modern sediments.

4.2.2. Moquegua sandstones

Detrital zircons from MoqA (Fig. 6h) and base of MoqB units (Fig. 7h) show dominantly Mesozoic cooling ages with only few Cenozoic ages. This largely reflects the previous observation made for MoqA and MoqC1 (in Cuno Cuno) quartzarenite pebble populations (Fig. 6f–g) and suggests a major provenance by recycling of non-reset fission track ages from Mesozoic sediments. This is also supported by the high proportion of transparent and rounded zircons. However, given that U–Pb ages clearly exclude a predominant Mesozoic source (see above), we have to consider that recycling of zircon from Paleozoic strata may produce similar ZFT spectra as observed for the Mesozoic pebble populations and outcrop samples. The small shift towards younger, i.e. Late Cretaceous–Tertiary

Table 2
Synopsis of the zircon fission track results. The upper part of the table shows the results obtained on the potential source formations, while the lower part presents the ZFT ages of the Moquegua sediments. The identification of age clusters was performed by the PopShare software (Dunkl and Székely, 2002). Abbreviations: pp: pebble population; N tot: total number of grains; N r: number of rounded grains. The percentages on the stratigraphic age column on the right indicate the proportion of the age clusters. The chi-square age was determined by the method of Brandon (1992).

Figure	Name	Lithology	Formation	Section	N tot	Nr	Chi-sq [%]	Disp
	COL-07-19	quartzarenite	modern pp	Majes	43	30	0	0.67
Fig. 6.a	MAJ-07-12	quartzarenite	modern pp	Majes	44	39	0	0.39
	MAJ-04-241	quartzarenite	outcrop	Majes	41	35	0	0.28
	YUR-08-01	quartzarenite	outcrop	Majes	44	36	0	0.34
Fig. 6.b	YUR-08-03	quartzarenite	outcrop	Majes	44	36	0	0.45
	OCO-07-33	quartzarenite	modern pp	Cuno Cuno	50	37	0	0.63
	OCO-08-03	quartzarenite	modern pp	Cuno Cuno	50	32	0	0.46
Fig. 6.c	VIT-10-01	quartzarenite	MoqD pp	Majes	42	40	0	0.47
Fig. 6.d	LOC-08-01	quartzarenite	MoqC (C2) pp	Moquegua	42	34	0	0.23
Fig. 6.e	MAJ-08-03	quartzarenite	MoqB pp	Majes	44	41	0	0.67
	LOC-08-04	quartzarenite	MoqB pp	Moquegua	44	39	0	0.85
Fig. 6.f	CUC-08-02	quartzarenite	MoqB pp	Cuno Cuno	44	36	0	0.72
Fig. 6.g	MAJ-10-01	quartzarenite	MoqA pp	Majes	43	43	0	0.67
Fig. 7.a	MAJ-07-03	gneiss	MoqD pp	Majes	25	20	0	0.64
Fig. 7.b	OCO-07-03	gneiss	modern pp	Cuno Cuno	33	13	0	0.44
Fig. 7.c	OCO-08-04	gneiss	modern pp	Cuno Cuno	25	10	0	0.84
Fig. 7.d	MAJ-07-04	sandstone	MoqD	Majes	54	16	100	1.17
	MOQ-10-02	sandstone	MoqD	Moquegua	70	53	100	1.02
	MAJ-07-40	sandstone	MoqC (C2)	Majes	81	12	100	0.73
Fig. 7.e	CUC-08-04	sandstone	MoqC (C2)	Cuno Cuno	68	27	0	0.63
	MOQ-04-218	sandstone	MoqC (C2)	Moquegua	36	0	0	0.26
Fig. 7.f	CUC-05-01	sandstone	MoqC (C1)	Cuno Cuno	80	44	100	0.9
Fig. 7.g	MAJ-10-02	sandstone	MoqB	Majes	81	72	0	0.67
	LOC-05-04	sandstone	MoqB	Moquegua	78	40	0	0.68
Fig. 7.h	MOQ-08-02	sandstone	base MoqB	Moquegua	50	34	0	0.66
Fig. 6.h	CARA-10-02	sandstone	MoqA	Caraveli	80	50	0	0.78
	MAJ-07-13	sandstone	base MoqA	Majes	63	44	0	0.38

Major age clusters and their weights

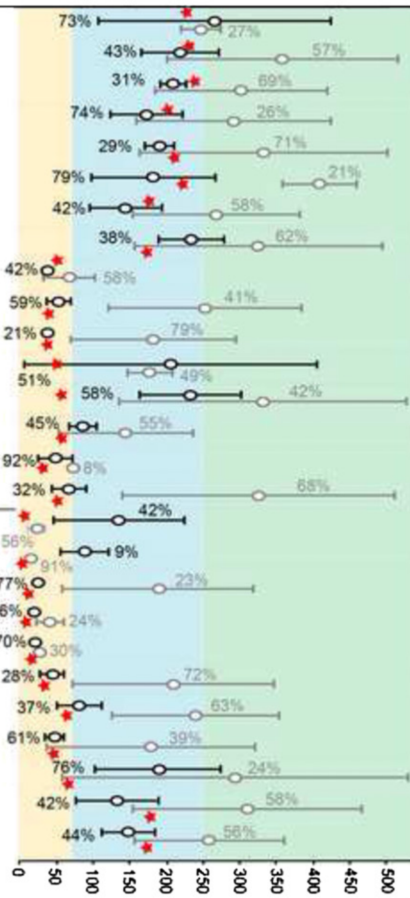

Cenozoic Mesozoic Paleozoic Chi-sq age younger age cluster older age cluster

cooling ages, especially in the base MoqB sample (Fig. 7h), highlights a further contribution from reset Arequipa Massif gneisses (Fig. 7a, c; supported by some pink and non-euhedral zircon grains) and/or Toquepala volcanic arc (91–45 Ma).

The ZFT ages of samples from MoqB (Fig. 7g) and MoqC1 (in Cuno Cuno) (Fig. 7f) show a major Paleogene age cluster around 48 Ma and 36 Ma, respectively, and the presence of many grains of Paleozoic to Mesozoic age. This indicates major provenance from the Toquepala volcanic arc (non-rounded zircons with Eocene age). In case of MoqC1 in Cuno Cuno, however, ages peaking around 36 Ma already point to the Andahuaylas–Anta volcanic arc (45–30 Ma; Mamani et al., 2010; see also U–Pb ages in 4.2.1). At this time, minor contributions from partially-reset Mesozoic sediments (Fig. 6e) and the metamorphic Arequipa Massif (pink rounded/angular zircons with Eocene ZFT age; Fig. 7a, b) are evident. Detrital zircons from MoqC2 (Fig. 7e) and MoqD units (Fig. 7d) have a dominant Miocene (~19 Ma) and Pliocene (~3 Ma) age cluster. Less than 10% of the ZFT ages are Paleozoic or Mesozoic. Both units contain 79% (MoqC2) and 44% (MoqD) non-rounded zircons reflecting a mainly volcanic provenance. In the case of MoqC2 unit the main provenance of volcanic zircons was the 24–10 Ma Huaylillas arc and for MoqD unit the main source was the 10–3 Ma Lower Barroso arc. The proportion of rounded grains in both units, however, point to varying contribution from reset Mesozoic sediments (Fig. 6d) for MoqC2 and non-reset Mesozoic sediments (Fig. 6c) for MoqD.

5. Discussion

Our data allow us (1) to reconstruct the provenance of the Mesozoic quartzarenites from the Arequipa–Tarapaca basin, (2) to refine the provenance scenario for the Cenozoic forearc sediments in southern Peru that was previously introduced by Decou et al. (2011), and (3) to develop a more detailed timing of the early Andean uplift and erosion in Southern Peru. We will first summarize the general provenance and age patterns for the Mesozoic and Cenozoic basins (Figs. 8 and 9) and then present their implications for the timing of the Central Andean uplift and a scenario to explain early crustal thickening (Fig. 10).

5.1. Provenance model

The Mesozoic sedimentary rocks of the Yura Group (mainly the quartzarenites) constitute an important source for the Cenozoic forearc sediments of Moquegua Group. Our new U–Pb data in combination with data on similar rocks from northern Chile (Wotzlaw et al., 2011) allow us to infer that Mesozoic sediments are derived from the Arequipa Massif as well as recycled Paleozoic

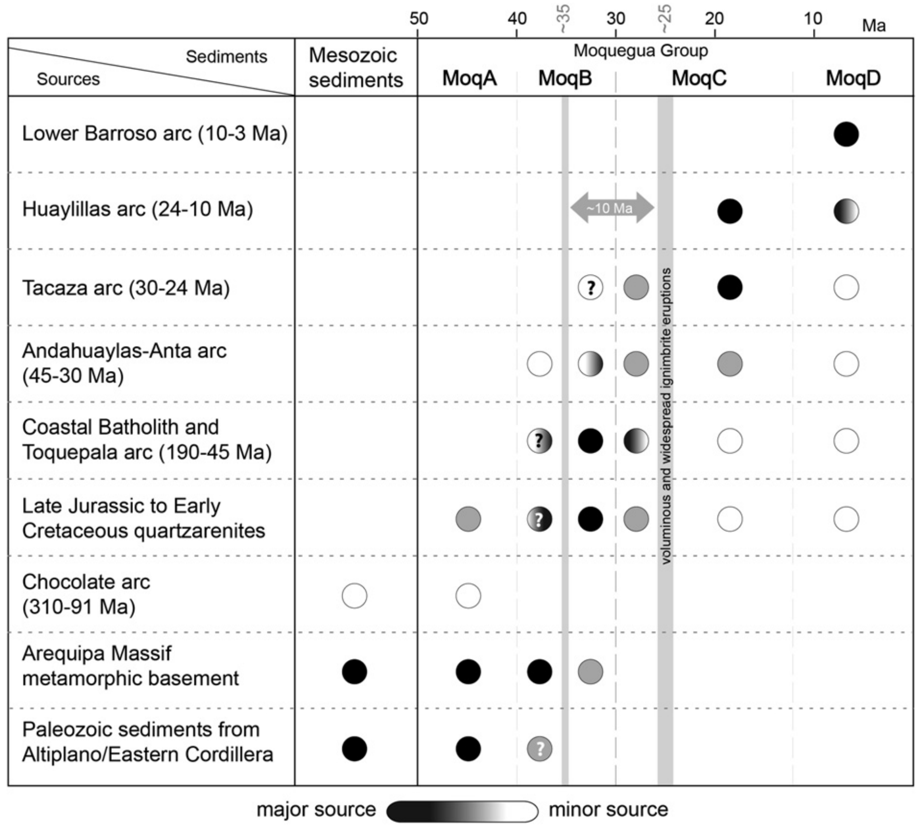

Fig. 8. Zircon-bearing source formations of the Mesozoic sediments and Moquegua units (A, B, C and D) based on the U–Pb zircon dating, zircon fission track ages and data from Decou et al. (2011) and Wotzlaw et al., 2011. The dames of the shading of the symbols corresponds to the estimated contribution of the sources in the sedimentary units. Ages indicated at the arcs are formation ages of the magmatites.

(mainly Ordovician) sedimentary rocks from the Eastern Cordillera and the Altiplano, along with a very minor contribution from the Triassic–Cretaceous Chocolate volcanic arc (Fig. 8). U–Pb data are consistent from Caravelí area (15.5°S) in Peru to Quebrada Guatacondo in northern Chile (21°S; Wotzlaw et al., 2011) implying the existence of a large internally connected back-arc basin in the Late Jurassic to Early Cretaceous that was fed by a largely uniform source from the northwest.

Regarding the Cenozoic Moquegua basin, sediment provenance of each of the units is summarized and discussed in Fig. 8 and in the following paragraphs. U–Pb detrital zircon ages from the MoqA unit (∼50 to ∼40 Ma) highlight a provenance from Ordovician sediments from the Altiplano as well as Proterozoic Arequipa Massif basement gneisses (affected by the Famatinian event in Caravelí but not in Majes). Furthermore, Devonian sediments have contributed to MoqA sediments, either coming from local sources (Majes area) or from the Altiplano (Caravelí area). With respect to the Mesozoic sediments we have contrasting evidence. Previous data based on heavy minerals and single grain Fe–Ti oxide geochemistry were interpreted to reflect a major provenance from the Mesozoic (Decou et al., 2011). This is mainly corroborated by zircon shape and color pointing to significant contributions from recycled Mesozoic sediments during MoqA deposition. Moreover, conglomerate layers at the base of MoqA contain Mesozoic quartzarenite pebbles. The hardness of these pebbles, however, may lead to overestimating the contribution from that source. Our U–Pb dataset clearly shows that the Mesozoic sediments cannot be the major source for the MoqA unit. Moreover, zircon morphology and ZFT data in Moquegua sandstones that resemble those of Mesozoic sediments may also derive from zircon recycling from Paleozoic sediments with similar characteristics (see above, 4.2.2). In this light the observed Fe–Ti oxide geochemical similarities between MoqA unit and Mesozoic sediments are better explained by a common source for both formations, most likely the metamorphic basement for which many Fe–Ti oxide geochemical characteristics are similar to those of MoqA and Mesozoic sediments (Decou et al., 2011).

Detrital ZFT ages from base MoqB show a major provenance from partially thermally reset Mesozoic sediments (Jurassic age cluster). The late Cretaceous–Paleogene ZFT ages most likely indicate a contribution from the 91–45 Ma Toquepala arc as well as from the thermally reset Arequipa Massif basement gneisses (ZFT ages were reset during the 91–45 Ma Toquepala volcanic arc activity) in agreement with single grain amphibole and Fe–Ti oxide geochemistry (Decou et al., 2011). Detrital zircon U–Pb and ZFT ages from the middle to upper part of MoqB unit emphasize a major provenance from partially-reset Mesozoic sedimentary rocks as well as from Arequipa Massif basement gneisses with a contribution from 91 to 45 Ma Toquepala arc, which is significant in the Majes area. Additionally, at Cuno Cuno and Locumba (Moquegua section) we found a large amount of non-rounded zircons with 45–30 Ma Andahuaylas–Anta arc ages. This indicates provenance from this arc which is in agreement with amphibole geochemistry (Decou et al., 2011). Our detrital zircon U–Pb and ZFT data together with heavy mineral petrography and single grain geochemistry (Decou et al., 2011) of MoqB (Fig. 8) reveals two significant changes of provenance within the unit. The first provenance change is observed at ∼40 Ma (MoqA/MoqB boundary) when detrital material in the Moquegua Group was no longer sourced from the distal Eastern Cordillera and the Altiplano. The second major provenance

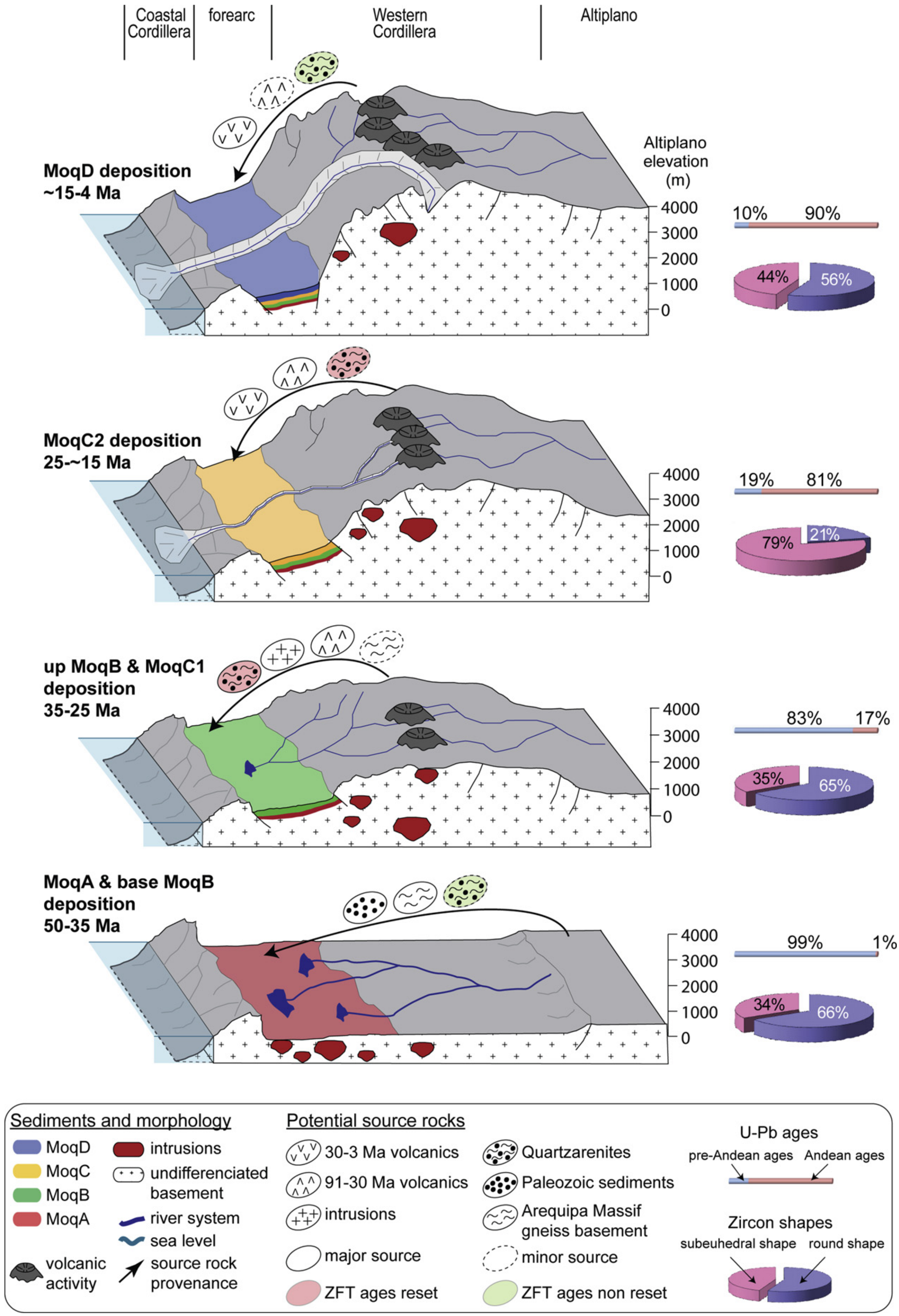

Fig. 9. Block diagram representing the timing of the Andean uplift, inferred from our provenance model, along an W-E profile drawn according to Gregory-Wodzicki (2000), Anders et al. (2002), Garzione et al. (2008) and Sempere and Jacay (2008) on the left side. On the right side are represented the proportions of pre-Andean to Andean ages as well as the zircon shape. ZFT: zircon fission track.

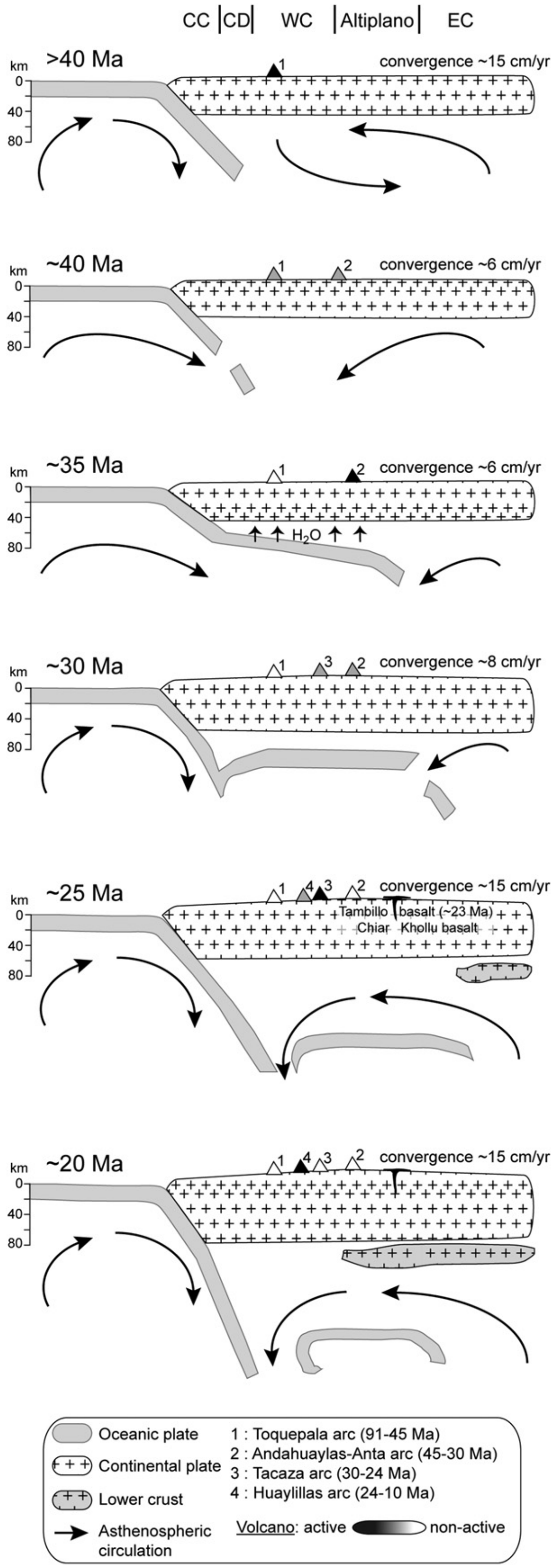

Fig. 10. Sketches illustrating a possible scenario of large-scale crustal processes leading to crustal thickening below the Central Andes beginning at around 35-30 Ma.

break occurred during MoqB deposition and can be tentatively placed at ~35 to >30 Ma, a time from which detrital material was overwhelmingly and directly derived from Toquepala arc rocks (91–45 Ma) and partially reset Mesozoic rocks, as well as from the contemporaneous active volcanic arc rocks (45–30 Ma Andahuaylas–Anta arc).

Detrital zircon U–Pb and ZFT ages from MoqC (30 to ~15–10 Ma) and MoqD (~15–10 to 4 Ma) units clearly identify a provenance from the different contemporaneous active volcanic arcs. The 30–24 Ma Tacaza and 24–10 Ma Huaylillas arcs signatures are largely present in MoqC unit whereas both are only minor in MoqD. The 10–3 Ma Lower Barroso arc is the dominant source for the MoqD unit. In addition, our data show a minor contribution from the 91–45 Ma Toquepala arc (MoqC unit) and Mesozoic sediments (Decou et al., 2011).

Regarding the thermal resetting of the ZFT thermometer in the source rocks we suggest the following scenario: The ZFT data show that the Arequipa Massif basement gneiss ages were partially to totally reset due to intrusive bodies related to the Toquepala arc (91–45 Ma) and its related volcanic arc activity. During sedimentation of MoqA and early MoqB, thermally unaffected Mesozoic (or Paleozoic) sediments were also eroded. The deposition of the middle part of MoqB unit coincides with the onset of uplift and activity of associated faults at the margin of the Western Cordillera (Isacks, 1988; Allmendinger et al., 1997), which exhumed 91–45 Ma old plutonic rocks of the Toquepala arc along with their Mesozoic host rocks. These intrusions partially and/or totally reset the ZFT ages of the surrounding Mesozoic sediments, which became the source of middle MoqB to MoqC units. Moreover, Decou et al. (2011) showed, using single grain amphibole and Fe–Ti oxide geochemistry, that the Toquepala volcanic arc (91–45 Ma) becomes a source during MoqB unit deposition. This is clearly confirmed here by our U–Pb data of upper MoqB in Majes. The first Eocene pulse of the Andean uplift (Isacks, 1988; Allmendinger et al., 1997) coincides with the sedimentation period of the middle to upper part of MoqB unit. A second pulse of uplift (Schildgen et al., 2007; Thouret et al., 2007; Garzione et al., 2008; Sempere and Jacay, 2008; Schildgen et al., 2009) occurred during MoqD sedimentation and exposed Mesozoic sediments to the surface which were not thermally affected by the 91–45 Ma old Toquepala arc plutons. The variable thermal reset, of the ZFT ages in the source areas reflects plutonic bodies that intruded locally and spatially separated into the Mesozoic sedimentary rock strata. Penetrative heating of the crust and homogeneous heat flow from the 91–45 Ma Toquepala volcanic arc activity is not observed.

The MoqA unit shows distal provenance from Paleozoic sediments now exposed on the Altiplano with contribution of the Arequipa Massif. Moreover, the fine-grained MoqA sediments starting at ~50 Ma reflect a low-energy lacustrine depositional environment and low relief (Fig. 9). The region of the present Altiplano was around sea level from end of Cretaceous until at least 60 Ma as indicated by the shallow marine deposits of the Molino Formation (Sempere et al., 1997). This comparatively quiet tectonic situation was followed by major tectonic activity leading to initial uplift of the Altiplano and Eastern Cordillera between 46 and 38 Ma (Horton et al., 2001; Anders et al., 2002; Horton et al., 2002; Gillis et al., 2006; Barnes et al., 2008; Sempere et al., 2008). The thick conglomerate layers observed in MoqB and along the MoqB to MoqC boundary (base of C1) deposits indicate fluvial systems which had much higher energy. At the same time, our provenance analysis of MoqB deposit shows no more contributions from the Ordovician to Devonian sediments from distal eastern sources (rocks now exposed on the Altiplano and further east), and a decrease of contribution from Arequipa Massif. This suggests that the onset of the formation of relief is also reflected in a reorganization of the drainage system on the western flank of the growing Andean belt. Apparently, at this time, i.e. during middle to upper MoqB sedimentation the sources from the Eastern Cordillera and Altiplano where cut off by tectonic processes (Fig. 9). The onset of this major change in sediment provenance and drainage system can thus be estimated between ∼35 Ma and 30 Ma at the latest. The establishment of this new drainage system was largely completed at ∼25 Ma at the time of the emplacement of widespread ignimbrite volcanism in the area (Wörner et al., 2000a; Thouret et al., 2007; Mamani et al., 2010). A similar change in source area and drainage systems was observed in northern Chile (Wotzlaw et al., 2011). This implies that large-scale phenomena such as climate change or deep-seated crustal processes are required to explain the 5–10 Ma lag time between shortening-induced change of relief and drainage systems, and voluminous volcanism. It is largely accepted that the Humboldt Current, which was established after the opening of the Drake Passage at ∼40 Ma (Staudigel et al., 1985; Scher and Martin, 2006), is responsible for the arid climate on the western margin of the Central Andes. Thus, we expect a trend towards increasing aridity during MoqB sedimentation which is in contradiction with the observed facies changes towards higher energy fluvial systems (Decou et al., 2011). Therefore, the provenance changes within MoqB are most likely related to tectonic processes and not to climate effects.

5.2. Changes in crustal processes

The up to ∼10 Ma lag time between uplift-related provenance changes initiated at ∼35 to >30 Ma and major voluminous ignimbrite eruptions starting at ∼25–22 Ma indicates that magmatism is not the main driving factor for crustal thickening at that time (Wörner et al., 2002; Decou et al., 2011). If magmatic addition would be the major driver for crustal thickening at that time, the implied volume increase in the Andean crust magmatism would be in the order of a flood basalt province (Wörner et al., 2002) with abundant mafic rocks, which is not observed in the study area.

The period of change, lasting 5–10 Ma, coincides with major vertical-axis tectonic rotations in southern Peru (Roperch et al., 2006) and an episode of flat subduction (Scheuber et al., 2006) followed by a strong acceleration of convergence rate during Oligocene time (Somoza, 1998). According to Gutscher (2000, 2002) the primary factor controlling subduction style is the buoyancy effect of anomalously thick (15–20 km) oceanic crust (however, see Doglioni et al., 2007 for a contrasting view). During flat subduction the hot asthenospheric wedge moves away from the trench to the East, the coupling between the plates strongly increases which results in upper plate shortening (Martinod et al., 2010), and volcanism ceases (Scheuber et al., 2006). In this situation, the cold mantle between the Andean crust and flat slab will be serpentinised rather than melted (Bostock et al., 2002; Ranero and Sallares, 2004). This serpentinised mantle will acquire a density typical of continental crustal rocks which may lead up to ∼15–20% of “pseudo” crustal thickening (Giese et al., 1999). Based on such a scenario, we develop a model for the initial phase of thickening and uplift of the Andean crust as a consequence of flat slab subduction (Fig. 10).

Before 40 Ma, a steep subduction regime existed at the Andean margin with a high convergence rate of ∼15 cm/yr (Somoza, 1998) and volcanic activity as documented by the 91–45 Ma Toquepala arc. At ∼40 Ma the convergence rate decreased to ∼6 cm/yr, and remained low until ∼35 Ma (Somoza, 1998) probably coeval with the initiation of flat subduction and the passage of the Juan Fernandez aseismic ridge (Yanez et al., 2001). As demonstrated by Gutscher et al. (2000), Gutscher (2002) and (Martinod et al., 2010) flat subduction involves strong interplate coupling (decrease of the convergence rate) and low volcanic activity, as reflected by the volumetrically less important 45–30 Ma Andahuaylas–Anta arc activity far to the NE in a back arc position at that time (Mamani et al., 2010). Assuming an initial crustal thickness of 40 km at ∼35 Ma and an increase of ∼15%–20% of crustal-like low-density rocks due to serpentinisation processes in the mantle wedge below the crust (Giese et al., 1999; i.e. 2.8 g/cm^3 compared to 3.3 g/cm^3 for the non-serpentinised mantle) should result in isostatic uplift of about ∼1000 to ∼1400 m. This estimated range of uplift may well explain the major change in the drainage system at ∼35 to >30 Ma described above.

At ∼30 Ma, the convergence slightly increased to ∼8 cm/yr (Somoza, 1998). During this time the subducted slab starts to steepen again. The change from flat slab to steep subduction plate between ∼30 and ∼25 Ma coincides with an increase in the plate convergence rate to ∼15 cm/yr that persists until ∼20 Ma (Somoza, 1998, Fig. 10). Mantle flow models (Espurt et al., 2008; Perez-Gussinye et al., 2008), however, indicate that such changes in slab angle cannot be accommodated in such short time by simply changing the dip of the subducted lithosphere. We therefore propose a slab break between the flat slab and a re-initiation of steep subduction at the trench. As a consequence, steep-slab subduction and its related magmatism can be re-established relatively quickly (within a few Ma) resulting in the establishment of the Tacaza arc at 30–24 Ma. The flat slab may remain in a critically buoyant state before it later starts to sink down into the mantle. This lithosphere sinking allows hot asthenospheric material to enter below the Andean crust resulting in the formation of mafic magmas below the Altiplano (around 23 Ma, Tambillo and Chiar Khollu back arc basalts in Bolivia; Lamb and Hoke, 1997). This led to an increase in magma production, heating of the lower crust and, eventually, the voluminous ignimbrite eruptions around 25–22 Ma (Lamb and Hoke, 1997; Wörner et al., 2002; Thouret et al., 2007).

Since ∼20 Ma the convergence progressively decreased to the present-day rate of ∼8 cm/yr (Somoza, 1998). Asthenospheric circulation allowed for (i) further steepening of the slab, illustrated at the surface by the back-migration of the active volcanic arc towards the trench (Mamani et al., 2010) and (ii) the flow of lower crust from east to west (Husson and Sempere, 2003). The flow of the lower crustal material explains the volume deficit under the Altiplano and Western Cordillera where the crust is thick without shortening (Wörner et al., 2002; Husson and Sempere, 2003).

6. Conclusions

Previously published provenance models for the Cenozoic forearc sediments in southern Peru (Decou et al., 2011) and northern Chile (Wotzlaw et al., 2011) are substantiated and refined using zircon U–Pb and fission track data, and are interpreted towards their implications for the timing of early uplift of the Central Andes and the underlying large-scale crustal processes.

At the time of MoqA sedimentation (∼50 to ∼40 Ma) detritus is derived from Proterozoic Arequipa Massif basement gneisses and Ordovician sediments from the Altiplano. Minor contributions come from erosion of Devonian sediments, either coming from local sources (Majes area) or from the Altiplano (Caravelí area), as well as Mesozoic sedimentary rocks of the Yura Group. Within the MoqB unit two significant breaks in sediment provenance are documented. The first break is observed at ∼40 Ma (MoqA/MoqB boundary) when detrital material from the Eastern Cordillera and Altiplano is no longer delivered to the Moquegua basin. The second major break in provenance occurred during MoqB deposition at approximately 35 to >30 Ma when exhumed Toquepala arc intrusives and their Mesozoic host rocks became major sources along with some contribution from the contemporaneous active volcanic arc (Andahuaylas–Anta arc). Detrital zircon U–Pb and ZFT ages from MoqC (30–∼15–10 Ma) and MoqD (∼15–10 to 4 Ma) units highlight major provenance from the respective volcanic arcs active during sedimentation. Moreover, our data still show minor contributions from Toquepala arc rocks and Mesozoic strata. The latter are not reset with respect to ZFT in case of MoqD.

Fine-grained sediments from MoqA reflect lacustrine sedimentation with detrital material coming partly from the Altiplano and Eastern Cordillera. The depocenters were close to sea level implying low relief during MoqA sedimentation. The thick conglomerate layers observed in the middle part of MoqB (especially in Caravelí and Majes areas) indicate the onset of higher energy fluvial systems that coincides with cutting-off sediment delivery from the Altiplano. This is clear evidence for the formation of significant relief, followed by reorganization of the drainage system on the western flank of the growing Andean orogen. The phase of change in drainage system and sediment provenance started as early as ∼35 Ma and was largely completed at ∼25 Ma. It was followed by the emplacement of voluminous volcanism in the area.

The up to 10 Ma lag time between uplift-related provenance changes at ∼35 to >30 Ma and major voluminous ignimbrite eruptions starting at ∼25–22 Ma strongly supports that magmatic addition to the crust is not the main driving factor for crustal thickening in the central part of the Central Andean Orocline at that time. Instead, large-scale tectonic processes involving the subduction regime are suggested to control uplift that is roughly estimated to be in the range of about 1–1.4 km by isostasy assuming serpentinisation of cold mantle wedge material below Andean crust. The model integrates the coincidence of (i) the onset of provenance change no later than 35 Ma, (ii) a drastic decrease in convergence rates at ∼40 Ma, (iii) a flat-subduction period (∼40 to ∼30 Ma) leading to strong interplate coupling, and (iv) the strong decrease in volcanic activity between 45 and 30 Ma.

Acknowledgments

We thank Andreas Kronz for providing analytical support at the electron microprobe as well as Mirian Mamani, Thierry Sempere, Stefan Hoffmann, Victoria Haider and Guido Meinhold for fruitful discussions and multiple advices. We are grateful to the German Science Foundation (DFG) for funding this project through grants EY 23/14 to HvE and Wo 362/39 to GW.

Appendix A. Supplementary data

Supplementary data related to this article can be found at http://dx.doi.org/10.1016/j.jsames.2013.02.003.

References

Acosta, H., Alvan, A., Mamani, M., Oviedo, M., Rodriguez, J., 2011. Geología de los cuadrángulos de Pachía y Palca, hojas 36-v y 36-x, escala 1:50,000. INGEMMET Boletín. Serie A: Carta Geológica Nacional 139, 96.

Acosta, H., Mamani, M., Alván, A., Oviedo, M., Rodriguez, J., 2010. Análisis estructural y geoquímica en la solución de problemas cartográficos de rocas volcánicas del Jurásico, ejemplo de la Formación Junerata en el cerro Junerata. Palca-Tacna. XV Congreso Peruano de Geología. Sociedad Geologica del Perú, Cusco Peru. Resumenes Extendidos, pp. 746–749.

Allmendinger, R.W., Jordan, T.E., Kay, S.M., Isacks, B.L., 1997. The evolution of the Altiplano-Puna plateau of the Central Andes. Earth and Planetary Science Letters 25, 139–174.

Anders, M.H., Gregory Wodzicki, K.M., Spiegelman, M., 2002. A critical evaluation of late Tertiary accelerated uplift rates for the Eastern Cordillera, Central Andes of Bolivia. Journal of Geology 110, 89–100.

Babeyko, A.Y., Sobolev, S.V., Trumbull, R.B., Oncken, O., Lavier, L.L., 2002. Numerical models of crustal scale convection and partial melting beneath the Altiplano-Puna plateau. Earth and Planetary Science Letters 199, 373–388.

Bahlburg, H., Carlotto, V., Cardenas, J., 2006. Evidence of early to middle Ordovician arc volcanism in the Cordillera oriental and Altiplano of southern Peru, Ollantaytambo formation and Umachiri beds. Journal of South American Earth Sciences 22, 52–65.

Bahlburg, H., Hervé, F., 1997. Geodynamic evolution and tectonostratigraphic terranes of northwestern Argentina and northern Chile. Geological Society of America Bulletin 109, 869–884.

Bahlburg, H., Vervoort, J.D., Du Frane, S.A., Bock, B., Augustsson, C., Reimann, C., 2009. Timing of crust formation and recycling in accretionary orogens: Insights learned from the western margin of South America. Earth-Science Reviews 97, 215–241.

Barnes, J.B., Ehlers, T.A., McQuarrie, N., O'Sullivan, P.B., Tawackoli, S., 2008. Thermochronometer record of central Andean Plateau growth, Bolivia (19.5°S). Tectonics 27, TC3003. doi: 3010.1029/2007TC002174.

Beck, S.L., Zandt, G., 2002. The nature of orogenic crust in the central Andes. Journal of Geophysical Research – Solid Earth 107, 2230–2246.

Beck, S.L., Zandt, G., Myers, S.C., Wallace, T.C., Silver, P.G., Drake, L., 1996. Crustal-thickness variations in the central Andes. Geology 24, 407–410.

Bostock, M.G., Hyndman, R.D., Rondenay, S., Peacock, S.M., 2002. An inverted continental Moho and serpentinization of the forearc mantle. Nature 417, 536–538.

Brandon, M.T., 1992. Decomposition of fission-track grain-age distributions. American Journal of Science 292, 535–564.

Carrapa, B., 2010. Resolving tectonic problems by dating detrital minerals. Geology 38, 191–192.

Casquet, C., Baldo, E., Pankhurst, R.J., Rapela, C.W., Galindo, C., Fanning, C.M., Saavedra, J., 2001. Involvement of the Argentine Precordillera terrane in the Famatinian mobile belt: U–Pb SHRIMP and metamorphic evidence from the Sierra de Pie de Palo. Geology 29, 703–706.

Casquet, C., Fanning, C.M., Galindo, C., Pankhurst, R.J., Rapela, C.W., Torres, P., 2010. The Arequipa Massif of Peru: new SHRIMP and isotope constraints on a Paleoproterozoic inlier in the Grenvillian orogen. Journal of South American Earth Sciences 29, 128–142.

Cawood, P.A., 2005. Terra Australis Orogen: Rodinia breakup and development of the Pacific and Iapetus margins of Gondwana during the Neoproterozoic and Paleozoic. Earth-Science Reviews 69, 249–279.

Chew, D.M., Schaltegger, U., Kosler, J., Whitehouse, M.J., Gutjahr, M., Spikings, R.A., Miskovic, A., 2007. U–Pb geochronologic evidence for the evolution of the Gondwanan margin of the north-central Andes. Geological Society of America Bulletin 119, 697–711.

Clark, A.H., Farrar, E., Kontak, D.J., Langridge, R.J., Arenas, F., Mario, J., France, L.J., McBride, S.L., Woodman, P.L., Wasteneys, H.A., 1990. Geologic and geochronologic constraints on the metallogenic evolution of the Andes of southeastern Peru. Economic Geology 85, 1520.

Cordani, U.G., Sato, K., Teixeira, W., Tassinari, C.C.G., Basei, M.A.S., 2000. Crustal evolution of the South American platform. In: Tectonic Evolution of South America. 31st International Geological Congress, Rio de Janeiro, Brazil, pp. 19–40.

Cordani, U.G., Teixeira, W., D'Agrella-Filho, M.S., Trindade, R.I., 2009. The position of the Amazonian Craton in supercontinents. Gondwana Research 15, 396–407.

Decou, A., von Eynatten, H., Mamani, M., Sempere, T., Wörner, G., 2011. Provenance analysis of siliciclastic sediments from the Cenozoic Moquegua forearc basin of Southern Peru (15–18°S) based on heavy mineral petrography and geochemistry. Sedimentary Geology 237, 55–72.

Doglioni, C., Carminati, E., Cuffaro, M., Scrocca, D., 2007. Subduction kinematics and dynamic constraints. Earth-Science Reviews 83, 125–175.

Dumitru, T.A., 1993. A new computer-automated microscope stage system for fission-track analysis. International Journal of Radiation Applications and Instrumentation. Part D. Nuclear Tracks and Radiation Measurements 21, 575–580.

Dunkl, I., 2002. Trackkey: a Windows program for calculation and graphical presentation of fission track data* 1. Computers & Geosciences 28, 3–12.

Dunkl, I., Frisch, W., Kuhlemann, J., Brügel, A., 2009. Pebble population dating as an additional tool for provenance studies – examples from the Eastern Alps. Geological Society London Special Publications 324, 125–140.

Dunkl, I., Mikes, T., Simon, K., von Eynatten, H., 2008. Brief introduction to the Windows program Pepita: data visualization, and reduction, outlier rejection, calculation of trace element ratios and concentrations from LA–ICP-MS data. In: Sylvester, P. (Ed.), Laser Ablation ICP-MS in the Earth Sciences: Current Practices and Outstanding Issues. Mineralogical Association of Canada, Short Course, vol. 40, pp. 334–340.

Dunkl, I., Székely, B., 2002. Component analysis with visualization of fitting – PopShare, a Windows program for data analysis. Goldschmidt Conference Abstracts 2002, Geochimica et Cosmochimica Acta 66/15A, 201.

Espurt, N., Funiciello, F., Martinod, J., Guillaume, B., Regard, V., Faccenna, C., Brusset, S., 2008. Flat subduction dynamics and deformation of the South American plate: insights from analog modeling. Tectonics 27, 19.

Forsythe, R.D., Davidson, J., Mpodozis, C., Jesinkey, C., 1993. Lower Paleozoic relative motion of the Arequipa block and Gondwana; paleomagnetic evidence from Sierra de Almeida of northern Chile. Tectonics 12, 219–236.

Frei, D., Gerdes, A., 2009. Precise and accurate in situ U–Pb dating of zircon with high sample throughput by automated LA–SF-ICP-MS. Chemical Geology 261, 261–270.

Garzione, C.N., Hoke, G.D., Libarkin, J.C., Withers, S., MacFadden, B., Eiler, J., Ghosh, P., Mulch, A., 2008. Rise of the Andes. Science 320, 1304–1307.

Garzione, C.N., Molnar, P., Libarkin, J.C., MacFadden, B.J., 2007. Reply to Comment on "Rapid late Miocene rise of the Andean plateau: evidence for removal of mantle lithosphere" by Garzione et al. (2006). Earth and Planetary Science Letters 259, 630–633.

Giese, P., Scheuber, E., Schilling, F., Schmitz, M., Wigger, P., 1999. Crustal thickening processes in the Central Andes and the different natures of the Moho-discontinuity. Journal of South American Earth Sciences 12, 201–220.

Gillis, R.J., Horton, B.K., Grove, M., 2006. Thermochronology, geochronology, and upper crustal structure of the Cordillera Real: Implications for Cenozoic exhumation of the central Andean plateau. Tectonics 25, TC6007. doi: 6010.1029/2005TC001887.

Gleadow, A.J.W., 1981. Fission-track dating methods: what are the real alternatives? Nuclear Tracks 5, 3–14.

Gleadow, A.J.W., Hurford, A.J., Quaife, R.D., 1976. Fission track dating of zircon: improved etching techniques. Earth and Planetary Science Letters 33, 273–276.

Green, P.F., 1981. A new look at statistics in fission-track dating. Nuclear Tracks 5, 77–86.

Gregory-Wodzicki, K.M., 2000. Uplift history of the Central and Northern Andes: a review. Geological Society of America Bulletin 112, 1091–1105.

Gutscher, M.A., 2002. Andean subduction styles and their effect on thermal structure and interplate coupling. Journal of South American Earth Sciences 15, 3–10.

Gutscher, M.A., Spakman, W., Bijwaard, H., Engdahl, E.R., 2000. Geodynamics of flat subduction: seismicity and tomographic constraints from the Andean margin. Tectonics 19, 814–833.

Horton, B.K., Hampton, B.A., Lareau, B.N., Baldellon, E., 2002. Tertiary provenance history of the Northern and central Altiplano (Central Andes, Bolivia): a detrital record of plateau margin tectonics. Journal of Sedimentary and Petrology 72, 711–726.

Horton, B.K., Hampton, B.A., Waanders, G.L., 2001. Paleogene synorogenic sedimentation in the Altiplano plateau and implications for initial mountain building in the central Andes. Bulletin of the Geological Society of America 113, 1387–1400.

Hurford, A.J., 1998. Zeta: the ultimate solution to fission-track analysis calibration or just an interim measure. Advances in Fission-Track Geochronology 80, 19–32.

Hurford, A.J., Fitch, F.J., Clarke, A., 1984. Resolution of the age structure of the detrital zircon populations of two Lower Cretaceous sandstones from the Weald of England by fission track dating. Geological Magazine 121, 269–277.

Hurford, A.J., Green, P.F., 1983. The zeta age calibration of fission-track dating. Chemical Geology 41, 285–317.

Husson, L., Sempere, T., 2003. Thickening the Altiplano crust by gravity-driven crustal channel flow. Geophysical Research Letters 30, 1243. doi: 1210.1029/2002GL016877.

Isacks, B.L., 1988. Uplift of the Central Andean Plateau and bending of the Bolivian orocline. Geophysical Research 93, 3211–3231.

Jackson, S.E., Pearson, N.J., Griffin, W.L., Belousova, E.A., 2004. The application of laser ablation–inductively coupled plasma-mass spectrometry to in situ U–Pb zircon geochronology. Chemical Geology 211, 47–69.

Kay, R.W., Mahlburg-Kay, S., 1991. Creation and destruction of lower continental crust. Geologische Rundschau 80, 259–278.

Kay, R.W., Mahlburg Kay, S., 1993. Delamination and delamination magmatism. Tectonophysics 219, 177–189.

Kay, S.M., Coira, B.L., 2009. Shallowing and steepening subduction zones, continental lithospheric loss, magmatism, and crustal flow under the Central Andean Altiplano-Puna Plateau. In: Kay, S.M., Ramos, V.A., Dickinson, W.R. (Eds.), 2009. Backbone of the Americas: Shallow Subduction, Plateau Uplift, and Ridge and Terrane Collision, vol. 204. Geological Society of America Memoir, pp. 229–260.

Kolodner, K., Avigad, D., McWilliams, M., Wooden, J.L., Weissbrod, T., Feinstein, S., 2006. Provenance of north Gondwana Cambrian–Ordovician sandstone: U–Pb SHRIMP dating of detrital zircons from Israel and Jordan. Geological Magazine 143, 367–391.

Lamb, S., Hoke, L., 1997. Origin of the high plateau in the Central Andes, Bolivia, South America. Tectonics 16, 623–649.

Loewy, S.L., Connelly, J.N., Dalziel, I.W.D., 2004. An orphaned basement block: the Arequipa–Antofalla Basement of the central Andean margin of South America. Geological Society of America Bulletin 116, 171–187.

Lyon-Caen, H., Molnar, P., Suárez, G., 1985. Gravity anomalies and flexure of the Brazilian Shield beneath the Bolivian Andes. Earth and Planetary Science Letters 75, 81–92.

Mamani, M., Wörner, G., Sempere, T., 2010. Geochemical variations in igneous rocks of the Central Andean orocline (13°S to 18°S): Tracing crustal thickening and magma generation through time and space. Geological Society of America Bulletin 122, 162–182.

Martinod, J., Espurt, N., Guillaume, B., Husson, L., Roperch, P., 2010. Horizontal subduction zones, convergence velocity and the building of the Andes. Earth and Planetary Science Letters 299, 299–309.

Meissner, R., Mooney, W., 1998. Weakness of the lower continental crust: a condition for delamination, uplift, and escape. Tectonophysics 296, 47–60.

Miskovic, A., Schaltegger, U., 2009. Crustal growth along a non-collisional cratonic margin: a Lu-Hf isotopic survey of the eastern cordilleran granitoids of Peru. Earth and Planetary Science Letters 279, 303–315.

Miskovic, A., Spikings, R., Chew, D., Košler, J., Ulianov, A., Schaltegger, U., 2009. Tectonomagmatic evolution of Western Amazonia: geochemical characterization and zircon U–Pb geochronologic constraints from the Peruvian Eastern Cordilleran granitoids. Geological Society of America Bulletin 121, 1298–1324.

Molnar, P., Garzione, C.N., 2007. Bounds on the viscosity coefficient of continental lithosphere from removal of mantle lithosphere beneath the Altiplano and Eastern Cordillera. Tectonics 26, TC2013. doi: 2010.1029/2006TC001964.

Mukasa, S.B., 1986. Zircon U–Pb ages of super-units in the Coastal batholith, Peru: implications for magmatic and tectonic processes. Geological Society of America Bulletin 97, 241–254.

Najman, Y., 2006. The detrital record of orogenesis: a review of approaches and techniques used in the Himalayan sedimentary basins. Earth-Science Reviews 74, 1–72.

Nemchin, A.A., Cawood, P.A., 2005. Discordance of the U–Pb system in detrital zircons: implication for provenance studies of sedimentary rocks. Sedimentary Geology 182, 143–162.

Oncken, O., Hindle, D., Kley, J., Elger, K., Victor, P., Schemmann, K., 2006. Deformation of the Central Andean upper plate system—Facts, fiction, and constraints for plateau models. In: The Andes, pp. 3–27. (Chapter 1).

Otamendi, J.E., Vujovich, G.I., de La Rosa, J.D., Tibaldi, A.M., Castro, A., Martino, R.D., Pinotti, L.P., 2009. Geology and petrology of a deep crustal zone from the Famatinian paleo-arc, Sierras de Valle Fértil and La Huerta, San Juan, Argentina. Journal of South American Earth Sciences 27, 258–279.

Pardo-Casas, F., Molnar, P., 1987. Relative motion of the Nazca (Farallon) and South American plates since Late Cretaceous time. Tectonics 6, 233–248.

Perez-Gussinye, M., Lowry, A.R., Phipps Morgan, J., Tassara, A., 2008. Effective elastic thickness variations along the Andean margin and their relationship to subduction geometry. Geochemistry, Geophysics, Geosystems 9, Q02003. doi: 02010.01029/02007GC001786.

Pinto, L., Hérail, G., Fontan, F., de Parseval, 2007. Neogene erosion and uplift of the western edge of the Andean Plateau as determined by detrital heavy mineral analysis. Sedimentary Geology 195, 217–237.

Quang, C.X., Clark, A.H., 2005. Response of supergene processes to episodic Cenozoic uplift, pediment erosion, and ignimbrite eruption in the porphyry copper province of southern Peru. Economic Geology 100, 87–114.

Ramos, V.A., 1988. Late Proterozoic-early Paleozoic of South America: a collisional history. Episodes 11, 168–174.

Ranero, C.R., Sallares, V., 2004. Geophysical evidence for hydration of the crust and mantle of the Nazca plate during bending at the north Chile trench. Geology 32, 549–552.

Reimann, C.R., Bahlburg, H., Kooijman, E., Berndt, J., Gerdes, A., Carlotto, V., López, S., 2010. Geodynamic evolution of the early Paleozoic Western Gondwana margin 14°–17° S reflected by the detritus of the Devonian and Ordovician basins of southern Peru and northern Bolivia. Gondwana Research 18, 370–384.

Roperch, P., Sempere, T., Macedo, O., Arriagada, C., Fornari, M., Tapia, C., García, M., Laj, C., 2006. Counterclockwise rotation of late Eocene–Oligocene fore-arc deposits in southern Peru and its significance for oroclinal bending in the central Andes. Tectonics 25, TC3010. doi: 3010.1029/2005TC001882.

Scher, H.D., Martin, E.E., 2006. Timing and climatic consequences of the opening of Drake Passage. Science 312, 428.

Scheuber, E., Mertmann, D., Ege, H., Silva-González, P., Heubeck, C., Reutter, K.J., Jacobshagen, V., 2006. Exhumation and basin development related to formation of the Central Andean Plateau, 21 S. In: The Andes, pp. 285–301. (Chapter 13).

Schildgen, T., Hodges, K., Whipple, K., Pringle, M., van Soest, M., Cornell, K., 2009. Late Cenozoic structural and tectonic development of the western margin of the central Andean Plateau in southwest Peru. Tectonics 28, TC4007. doi: 4010.1029/2008TC002403.

Schildgen, T.F., Hodges, K.V., Whipple, K.X., Reiners, P.W., Pringle, M.S., 2007. Uplift of the western margin of the Andean plateau revealed from canyon incision history, southern Peru. Geology 35, 523–526.

Sempere, T., Butler, R.F., Richards, D.R., Marshall, L.G., Sharp, W., Swisher, C.C., 1997. Stratigraphy and chronology of Upper Cretaceous–lower Paleogene strata in Bolivia and northwest Argentina. Geological Society of America Bulletin 109, 709–727.

Sempere, T., Carlier, G., Soler, P., Fornari, M., Carlotto, V., Jacay, J., Arispe, O., Néraudeau, D., Cardenas, J., Rosas, S., Jimerez, N., 2002. Late Permian middle Jurassic lithospheric thinning in Peru and Bolivia, and its bearing on Andean age tectonics. Tectonophysics 345, 153–181.

Sempere, T., Folguera, A., Gerbault, M., 2008. New insights into Andean evolution: an introduction to contributions from the 6th ISAG symposium (Barcelona, 2005). Tectonophysics 459, 1–13.

Sempere, T., Fornari, M., Acosta, J., Flores, A., Jacay, J., Pena, D., Roperch, P., Taipe, E., 2004. Estratigrafia, geocronologia, paleogeografia y paleotectonica de los depositos de antearco del sur del Peru, XII Congresso Peruano de Geologiá, Lima, Peru. (Abstract).

Sempere, T., Jacay, J., 2007. Synorogenic Extensional Tectonics in the Forearc, Arc and Southwest Altiplano of Southern Peru. AGU Joint Assembly, Acapulco. p. 04.

Sempere, T., Jacay, J., 2008. Anatomy of the Central Andes: distinguishing between western, magmatic Andes and eastern, tectonic Andes, 7th International Symposium on Andean Geodynamics, Nice, Abstract, pp. 504–507.

Shackleton, R.M., Ries, A.C., Coward, M.P., Cobbold, P.R., 1979. Structure, metamorphism an geochronology of the Arequipa Massif of coastal Peru. Journal of the Geological Society London 136, 195–214.

Sircombe, K.N., 2004. AgeDisplay: an EXCEL workbook to evaluate and display univariate geochronological data using binned frequency histograms and probability density distributions. Computers & Geosciences 30, 21–31.

Somoza, R., 1998. Updated azca (Farallon)—South America relative motions during the last 40 My: implications for mountain building in the central Andean region. Journal of South American Earth Sciences 11, 211–215.

Staudigel, H., Doyle, P., Zindler, A., 1985. Sr and Nd isotope systematics in fish teeth. Earth and Planetary Science Letters 76, 45–56.

Tassinari, C.C.G., Bettencourt, J.S., Geraldes, M.C., Macambira, M.J.B., Lafon, J.M., 2000. The Amazon craton. In: Tectonic Evolution of South America. 31st International Geological Congress, Rio de Janeiro, Brazil, pp. 41–95.

Thouret, J.C., Wörner, G., Gunnel, Y., Singer, B., Zhang, X., Souriot, T., 2007. Geochronologic and stratigraphic constraints on canyon incision and Miocene uplift of the Central Andes in Peru. Earth and Planetary Science Letters 263, 151–166.

Vicente, J.C., 1981. Elementos de la estratigraphia Mesozoica sur Peruana. In: Volkheimer, Musacchio (Eds.), 1981. Comité Sudamericano del Jurásico y Cretácico: Cuencas sedimentarias del Jurásico y Cretácico de America del sur, vol. 1, pp. 319–351.

Vicente, J.C., 1989. Early late Cretaceous overthrusting in the western cordillera of southern Peru. In: Ericksen, G.E., Canas Pinochet, M.T., Reinemund, J.A. (Eds.), Geology of the Andes and Its Relation to Hydrocarbon and Mineral Resources. Houston, Texas, Circum-pacific Council for Energy and Mineral Resources Earth Science Series, vol. 11, pp. 91–117.

Vicente, J.C., 2005. Dynamic paleogeography of the Jurassic Andean basin: pattern of transgression and localisation of main straits through the magmatic arc. Revista de la Asociación Geologíca Argentina 60, 221–250.

Vicente, J.C., 2006. Dynamic paleogeography of the Jurassic Andean basin: pattern of regression and general considerations on main features. Revista de la Asociación Geologíca Argentina 61, 408–437.

Vicente, J.C., Beaudoin, B., Chavez, A., Leon, I., 1982. La cuenca de Arequipa (sur Perú) durante el Jurássico-Cretácico inferior, In: V Congreso Latinoamericano de Geologia abstract volume (Ed. by ACTAS), Argentina, pp. 121–153.

von Eynatten, H., 2003. Petrography and chemistry of sandstones from the Swiss Molasse Basin: an archive of the Oligocene to Miocene evolution of the central Alps. Sedimentology 50, 703–724.

Wilson, J., García, W., 1962. Geología de los Cuadrángulos de Pachia y Palca. Comisión de la Carta Geológica Nacional 2 (4), 1–81.

Wörner, G., Hammerschmidt, K., Henjes-Kunst, F., Lezaun, J., Wilke, H., 2000a. Geochronology ($^{40}Ar/^{39}Ar$, K-Ar and He-exposure ages) of Cenozoic magmatic rocks from northern Chile (18–22° S): implications for magmatism and tectonic evolution of the central Andes. Revista Geológica de Chile 27, 205–240.

Wörner, G., Lezaun, J., Beck, A., Heber, V., Lucassen, F., Zinngrebe, E., Rössling, R., Wilke, H.G., 2000b. Precambrian and early Paleozoic evolution of the Andean basement at Belen (northern Chile) and Cerro Uyarani (western Bolivia Altiplano). Journal of South American Earth Sciences 13, 717–737.

Wörner, G., Uhlig, D., Kohler, I., Seyfried, H., 2002. Evolution of the western Andean Escarpment at 18°S (N. Chile) during the last 25 Ma: uplift, erosion and collapse through time. Tectonophysics 345, 183–198.

Wotzlaw, J.F., Decou, A., von Eynatten, H., Wörner, G., Frei, D., 2011. Jurassic to Paleogene tectono-magmatic evolution of northern Chile and adjacent Bolivia from detrital zircon U–Pb geochronology and heavy mineral provenance. Terra Nova 23, 399–406.

Yanez, G.A., Ranero, C.R., von Huene, R., Diaz, J., 2001. Magnetic anomaly interpretation across the southern central Andes (32 degrees–34 degrees S): the role of the Juan Fernandez Ridge in the late Tertiary evolution of the margin. Journal of Geophysical Research – Solid Earth 106, 6325–6345.

Yuan, X., Sobolev, S.V., Kind, R., 2002. Moho topography in the central Andes and its geodynamic implications. Earth and Planetary Science Letters 199, 389–402.